The Astrophysical Journal, 702:537–553, 2009 September 1 doi:10.1088/0004-637X/702/1/537

SOLAR WIND MAGNETOHYDRODYNAMICS TURBULENCE: ANOMALOUS SCALING AND ROLE OF INTERMITTENCY

C. Salem[1], A. Mangeney[2], S. D. Bale[1], and P. Veltri[3]
[1] Space Sciences Laboratory, University of California, Berkeley, CA 94720, USA; salem@ssl.berkeley.edu
[2] LESIA, Observatoire de Paris-Meudon, F-92195 Meudon, France
[3] Dipartimento di Fisica, Università della Calabria, Rende (Cs), Italy
Received 2009 January 9; accepted 2009 June 25; published 2009 August 13

ABSTRACT

In this paper, we present a study of the scaling properties and intermittency of solar wind MHD turbulence based on the use of wavelet transforms. More specifically, we use the Haar Wavelet transform on simultaneous 3 s resolution particle and magnetic field data from the *Wind* spacecraft, to investigate anomalous scaling and intermittency effects of both magnetic field and solar wind velocity fluctuations in the inertial range. For this purpose, we calculated spectra, structure functions, and probability distribution functions. We show that this powerful wavelet technique allows for a systematic elimination of intermittency effects on spectra and structure functions and thus for a clear determination of the actual scaling properties in the inertial range. The scaling of the magnetic field and the velocity fluctuations are found to be fundamentally different. Moreover, when the most intermittent structures superposed to the standard fluctuations are removed, simple statistics are recovered. The magnetic field and the velocity fluctuations exhibit a well-defined, although different, monofractal behavior, following a Kolmogorov −5/3 scaling and a Iroshnikov–Kraichnan −3/2 scaling, respectively. The multifractal properties of solar wind turbulence appear to be determined by the presence of those most intermittent structures. Finally, our wavelet technique also allows for a direct and systematic identification of the most active, singular structures responsible for the intermittency in the solar wind.

Key words: interplanetary medium – methods: data analysis – MHD – plasmas – solar wind – turbulence

Online-only material: color figures

1. INTRODUCTION

The solar wind is a collisionless plasma undergoing supersonic and super-Alfvénic spherical expansion. It provides a unique environment in which to study magnetohydrodynamics (MHD) turbulence in general, and in astrophysical plasmas in particular. Several heliospheric space missions have furnished the scientific community with a wealth of data (velocity, magnetic field, plasma density, temperature, etc. and also particle distribution functions) at a resolution which is not available in any terrestrial laboratory.

The solar wind plasma is strongly turbulent. One of the most striking features of the solar wind is indeed the very large number of degrees of freedom which are excited: the electromagnetic fields and plasma properties of the solar wind show fluctuations over a wide range of timescales ranging from the solar rotation period up to the local electron plasma period, i.e., frequencies f from 10^{-6} Hz to $f_{pe} \sim 2 \times 10^4$ Hz (Salem 2000).

For decades, many efforts have been put forward to understand the physical mechanisms of solar wind turbulence. Many fundamental issues have been addressed, such as the nature and the properties of the fluctuations, the origin and evolution of turbulence in the interplanetary medium, the mechanisms of the turbulent cascade of energy through the inertial range, and the corresponding "dissipation" at the smallest scales near the local ion gyrofrequency f_{ci}, and reviewed by numerous excellent papers (see Roberts & Goldstein 1991; Mangeney et al. 1991; Marsch 1991; Goldstein et al. 1995b; Goldstein 1995; Goldstein et al. 1997; Tu & Marsch 1995; Bruno 1997; Horbury 1999; Goldstein & Roberts 1999; Horbury et al. 2005; Bruno et al. 2005; Bruno & Carbone 2005). However, for reasons that we discuss below, two of the primary problems of solar wind MHD turbulence that still remain a puzzle are the nature of the nonlinear energy cascade and the strong intermittent character of solar wind fluctuations in the inertial range.

At MHD scales, i.e., for frequencies below the local ion gyrofrequency f_{ci} or length scales greater than the ion gyroradii, the solar wind plasma can be treated as a magnetofluid. Furthermore, the fluctuations may be assumed to be frozen in the supersonic, super-Alfvénic solar wind flow, so that spatial scales are translated in timescales for spacecraft data (Taylor's hypothesis). Solar wind MHD turbulence, just like neutral fluid turbulence (Frisch 1995), exhibits what appears to be an inertial domain at these scales, first noted by Coleman (1968), with power-law spectra and scale invariance, suggesting a nonlinear energy cascade from large "energy-containing" scales toward much smaller scales, where dissipation via kinetic effects is presumed to act. Typically, the observed inertial range at 1 AU extends over three decades of frequencies, from $f \sim 2 - 3\ 10^{-4}$ Hz up to $f \sim f_{ci}$ (a few tenths of Hz). In this range, the observed spectral slopes for magnetic field (e.g., Goldstein et al. 1995b; Bruno & Carbone 2005) and electric field (Bale et al. 2005) fluctuations in the inertial range are close to the value predicted by Kolmogorov (1941) for turbulence in non-conducting fluids.

Until the *Wind* spacecraft, solar wind plasma data (such as velocity, density, etc.) have in general had a much lower time resolution compared to magnetic field measurements, of the order of a few minutes (a few 10^{-2} Hz), so that only two decades of frequencies of velocity (or density) fluctuations could be explored in the inertial range, resulting in large uncertainties in their spectral slopes. The 3D-Plasma (3DP) experiment on board *Wind* (Lin et al. 1995) provides plasma data at a 3 s

resolution, thus allowing exploration of the inertial domain over three decades for velocity fluctuations. This showed that the scaling of the magnetic field and the velocity components are different, the spectral slope of velocity fluctuations being very close to 1.5, the Iroshnikov–Kraichnan prediction (Iroshnikov 1963; Kraichnan 1965). This difference was first observed by Salem (2000) and Mangeney et al. (2001) a few years ago, but the accuracy of the data were questioned. The 3DP plasma and the magnetic field data quality and precision have since been improved through better calibrations compared to the early part of the *Wind* mission without much of an effect on the results (Salem et al. 2007): the difference in scaling for the **B** and the **V** fields is even clearer (Salem et al. 2004, 2006, 2007). This trend does not depend on the type of spectral analysis used for the analysis. While the results by Salem (2000) and Mangeney et al. (2001) used a wavelet transform, they have been confirmed recently by Podesta et al. (2006a, 2007) using a standard Fourier transform.

Fluctuations in the solar wind as well as in developed neutral fluid turbulence (e.g., Frisch 1995), even if they display statistical homogeneity, are never purely scale invariant; in fact, their probability distribution functions (PDFs) change significantly going to small scales from the large scales, where they are more or less Gaussians. This property is known as *Intermittency* (e.g., Veltri et al. 2009). It may be seen, at small scales, as heavy tails in the PDFs of fluctuations. Intermittency is also responsible for departures from the scale invariance (or self-similarity) in the inertial range predicted by simple phenomenologies of turbulence (e.g., Frisch 1995; Biskamp 1993, 2003). For example, the K41 phenomenology in neutral fluid turbulence predicts that the fluctuations are self-similar, i.e., that the velocity fluctuation δv_ℓ at scale ℓ and its moments have the monofractal scaling law

$$\langle|\delta v_\ell|\rangle \propto \ell^h\ , \quad \langle|\delta v_\ell|^p\rangle \propto \ell^{\zeta(p)}\ , \quad p = 1, 2, \ldots,$$

the Hölder exponent $h = 1/3$ being a constant and $\zeta(p) = p\,h$, the average $\langle\ldots\rangle$ being taken over space; in this case, the Hölder exponent is also called the Hurst exponent ($h = H =$ constant). At variance with these predictions, observations show that the scaling exponent $\zeta(p)$ deviates from linearity and that it is a concave function of p. The multifractal formalism was introduced in the mid-eighties in order to understand these discrepancies, the basic idea being that the Hölder exponent is not really constant in space but actually depends on the location

$$|\delta v_\ell(x)| \propto \ell^{h(x)}. \tag{1}$$

Then $h(x)$ quantifies the local regularity (or strength of the "singularity") of the observed fields (Halsey et al. 1986) at the point x: when $h(x)$ is close to 0, the field is very irregular (or singular) at the point x, while larger values of $h(x)$ are related to a smoother (more regular) behavior at x.

At the difference from "monofractals," multifractal processes exhibit an intricate pattern of local regularity, and the set of points (or times) $\Omega(h)$ at which the process has a given Hölder exponent h is itself a fractal set with fractal (or Hausdorff) dimension $D(h)$; $D(h)$ is often referred to as the spectrum of singularities, and describes the relative frequency of occurrence of local abrupt fluctuations (singularities) with strength h. It provides a statistical and global description of the variations of "regularity" of the fields. The "multifractal" analysis aims at characterizing the statistics of the spatial distribution of local Hölder exponents with the singularity spectrum $D(h)$, related to the scaling exponent $\zeta(p)$ by a Legendre transformation (see Parisi & Frisch 1985).

Intermittency in the solar wind turbulence has been widely reported in the literature (Burlaga 1991, 1993; Marsch & Liu 1993; Marsch & Tu 1994; Carbone et al. 1995a, 1995b, 1996a, 1996b, 2004; Ruzmaikin et al. 1995; Horbury et al. 1996, 1997; Horbury & Balogh 1997; Bruno et al. 1999a, 1999c, 2003, 2007a, 2007b; Veltri & Mangeney 1999; Veltri 1999, 2004; Veltri et al. 2005, 2009; Pagel & Balogh 2002, 2003; Sorriso-Valvo et al. 2001, 2005). Most of these studies were centered around characterizing the multifractal nature of solar wind (mainly magnetic field) fluctuations. They focused on quantifying the departure from Gaussian statistics by analyzing PDFs or characterizing the anomalous scaling of structure functions and quantifying deviations from self-similarity by fitting different intermittency models to observed structure function curves (see Section 2 for more details). As will be discussed in the next section, this kind of approach, aimed at understanding the behavior of intermittent systems in turbulence, is purely statistical or geometrical, with no definitive model dominating the others and therefore no consistent way to quantify intermittency. Such geometrical models do not provide any information on the physics of intermittency, its physical nature, and how it affects the properties of solar wind turbulence in general.

In particular, the physical nature of the intermittent bursts of strong activity in developed turbulence is not yet fully understood. It is conjectured that part or all bursty contributions to turbulent fluctuations are in fact due to the spatially localized coherent structures observed in fully developed turbulence, which emerge from the surrounding background flow due to the nonlinearity of the flow dynamics. It is expected that these small-scale structures are related to the universal properties of turbulence, thereby exhibiting a generic geometric signature that may be characteristic of the cascade dynamics. Therefore, a characterization of these structures could hopefully provide a better understanding of cascade mechanics.

Soon after the introduction of the multifractal picture of fully developed turbulence, a wavelet-based statistical approach was proposed as a unified multifractal description of singular measures and multi-affine functions (e.g., Muzy et al. 1993, 1994). The ability of wavelets to provide good time resolution with modest frequency resolution matches well with the character of the broadband spectra typical of turbulent data. The usefulness of wavelets comes from a result by Meyer (1998) showing that, under mild regularity conditions on the process $\delta v_\ell(x)$, its local Hölder exponent $h(x)$ as defined in Equation (1) can be calculated from its wavelet coefficients $w(s,x)$ (s is the scale, see the definition in Section 3.2; see also Arneodo et al. 1988; Bacry et al. 1991; Farge 1992; Mimouni et al. 1995) which scale as the fluctuation $\delta v_\ell(x)$,

$$w(s, x) \sim s^{h(x)}, \tag{2}$$

independently of the chosen wavelet transform, provided that the analyzing wavelet is admissible and is sufficiently localized.

A wavelet analysis method for multifractal signals is therefore very efficient to extract local exponents and detect singularities in turbulent flows, allowing for their characterization. It also eliminates artifacts in the determination of the scaling $\zeta(p)$, redefining the structure functions in terms of wavelet transforms instead of linear increments (Arneodo et al. 1995; Bacry et al. 1993). It has proven to be an efficient way to determine statistical properties of complex systems, and to provide a good basis to analyze their geometry.

In the present study, we adopt a similar approach to study solar wind MHD turbulence using high-time resolution data from the *Wind* spacecraft at 1 AU. We use the Haar Wavelet transform on simultaneous *Wind* 3 s resolution particle and magnetic field data from the 3DP and the MFi experiments respectively, to investigate anomalous scaling and intermittency effects of both magnetic field and solar wind velocity fluctuations in the inertial range.

2. CHARACTERIZING ENERGY CASCADE AND INTERMITTENCY IN TURBULENCE

In the absence of a well accepted theory of turbulence, a number of phenomenological models have been developed in Fluid dynamics and/or MHD to understand the observed intermittency and scaling properties of fully developed turbulence.

2.1. Basic Phenomenologies

In phenomenological models for the turbulent cascade in an incompressible neutral fluid, the flow is considered to result from the superposition of "eddies" with sizes $\ell \leqslant L$, and associated velocity fluctuation $\delta v_\ell \sim |\mathrm{v}(r+\ell) - \mathrm{v}(r)|$. L is the largest (the outer scale) of the turbulent eddies. In incompressible MHD, one has also to consider the magnetic fluctuation $\delta B_\ell \sim |\mathrm{B}(r+\ell) - \mathrm{B}(r)|$.

In the usual picture of turbulence, the interaction between eddies makes the kinetic (plus eventually magnetic) energy $E(\ell) = \rho\,\delta v_\ell^2 + \delta B_\ell^2/2\mu_0$ cascade nonlinearly from large to small length scales, with a typical timescale $\tau_{tr}(\ell)$. This applies in the so-called inertial range, at scales smaller than the energy containing range ($\ell \simeq L$) but larger than the dissipation range where viscosity (or other dissipative effects) becomes the dominant physical effect (e.g., Frisch 1995). To describe the cascade in the inertial range, two main assumptions are used: (1) significant energy exchanges between eddies occur only between eddies of similar scales and (2) the rate ε of energy exchange between eddies is independent of their scale,

$$\varepsilon = \frac{E}{\tau_{tr}} = \text{independent of } \ell. \tag{3}$$

Different phenomenological models result from making various assumptions concerning the dominant contributions to E and τ_{tr} (e.g. Galtier et al. 2005; Müller & Biskamp 2003). The first one is the analogous of the *Kolmogorov* phenomenology (Kolmogorov 1941, 1962) for fluid turbulence (K41 hereafter). The turbulent eddies are assumed to be isotropic with normalized velocity and magnetic fluctuations of the same order of magnitude,

$$\frac{\delta v_\ell}{v_A} \sim \frac{\delta \mathrm{B}_\ell}{\bar{B}}, \tag{4}$$

where v_A is the Alfvén velocity associated to $\bar{B}$. Then the only available timescale is the characteristic nonlinear or eddy turnover time, $t_\ell \sim \ell/\delta v_\ell$, during which the eddy gives almost all of its energy $E \sim \delta v_\ell^2$ to eddies of smaller scales. Thus,

$$\tau_{tr} \sim t_\ell, \tag{5}$$

so that one obtains immediately

$$\delta v_\ell \propto \varepsilon^{1/3}\, \ell^{1/3}. \tag{6}$$

The scaling of the spectral energy density E_k can be obtained from the Bessel–Parseval theorem ($\int dk\, E_k \approx \delta v_\ell^2$, with $k \sim \ell^{-1}$), so that

$$E_k \approx \ell\ \delta v_\ell^2 \propto \varepsilon^{2/3}\, k^{-5/3}. \tag{7}$$

The second phenomenology, proposed independently by Iroshnikov (1963) and Kraichnan (1965, IK hereafter) is a variant of K41 that accounts for the propagation of the eddies in the large-scale magnetic field $\bar{\mathbf{B}}$ (*Alfvén effect*). Within this framework, the fluctuations are still assumed to be essentially isotropic but most of the energy transfer from scales to scales is due to interactions between Alfvénic type of fluctuations moving in opposite direction along $\mathbf{B}$ with the Alfvén speed v_A; this limits the time during which two eddies interact, which is on the order of an Alfvén time $t_A \sim \ell/v_A \ll t_\ell$ only, and thus increases the energy transfer time by a factor t_ℓ/t_A (Dobrowolny et al. 1980; Biskamp 1993),

$$\tau_{tr} \sim t_\ell\, \frac{t_\ell}{t_A}. \tag{8}$$

Under assumption (4), both δv_ℓ and δB_ℓ, and $E \sim \delta v_\ell^2$ should then obey the scaling

$$\delta v_\ell \propto \delta B_\ell \propto (\varepsilon\ v_A)^{1/4}\ \ell^{1/4}, \tag{9}$$

or

$$E_k \propto (\varepsilon\ v_A)^{1/2}\ k^{-3/2}. \tag{10}$$

However, both observations and numerical simulations indicate that the assumption of isotropy of MHD fluctuations must be relaxed (see, e.g., Müller & Biskamp 2003). In the presence of a large-scale average magnetic field $\bar{\mathbf{B}}$, the eddies become anisotropic with scales ℓ transverse to $\bar{\mathbf{B}}$ and λ parallel to $\bar{\mathbf{B}}$, $\lambda > \ell$. Goldreich & Sridhar (1995) proposed a phenomenology where the eddies are elongated along the average magnetic field $\bar{\mathbf{B}}$, $\lambda \gg \ell$, and the fluctuations essentially orthogonal to $\bar{\mathbf{B}}$, the perpendicular components $\delta v_\ell^\perp \sim \delta b_\ell^\perp$ being much larger than the parallel components (see also Goldreich & Sridhar 1997; Goldreich 2001). The shape of the eddies is fixed by a condition of "critical balance" $t_\ell \sim t_A$ between the eddy turn over time $t_\ell \sim \ell/\delta v_\ell^\perp$ and the Alfvèn time $t_A \sim \lambda/v_A$, so that the nonlinear transfer time τ_{tr} given by Equation (8) now becomes

$$\tau_{tr} \sim t_\ell \sim t_A, \tag{11}$$

i.e., the energy transfer time is on the order of the "perpendicular" eddy turn over time, which is itself of the order of the Alfvèn time needed for two interacting counter-propagating eddies to cross each other along the large-scale magnetic field.

Since $E \sim \left(\delta v_\ell^\perp\right)^2$, a Kolmogorov type of scaling is obtained ($k_\perp \sim 1/\ell$, $k_\parallel \sim 1/\lambda$),

$$E_{k_\perp, k_\parallel} \propto \varepsilon^{2/3}\ k_\perp^{-5/3}, \tag{12}$$

with eddy shapes $\lambda \propto \ell^{2/3}$ resulting from the critical balance condition.

All these phenomenologies do not appear to be entirely successful in explaining the results of the most recent numerical simulations (e.g., Müller et al. 2003; Mason et al. 2008). Indeed, these simulations show that the turbulent spectrum depends on the strength of the average magnetic field $\bar{\mathbf{B}}$, as measured by the ratio $\Gamma = \bar{B}^2/\rho\,\delta v_L^2$, where ρ is the mass density and δv_L is the velocity fluctuation at the largest scale. For small average magnetic field $\Gamma \ll 1$, the spectrum is the one predicted by Goldreich and Sridhar's anisotropic phenomenology (Goldreich

& Sridhar 1995), while for large average magnetic field $\Gamma \gg 1$, it is the anisotropic Iroshnikov–Kraichnan spectrum

$$E_{k_\perp,k_\parallel} \propto k_\perp^{-3/2}, \tag{13}$$

that best describes the results. Moreover, when $\Gamma \ll 1$, magnetic energy is significantly larger than kinetic energy at large scales, whereas they remain almost equal in the strong field case, $\Gamma \gg 1$ (see Müller & Grappin 2005).

2.2. Intermittency and Higher-order Statistics

The statistics of a variable $\delta\phi$ with a Gaussian PDF is fully determined by its variance (second order moment of the PDF). However, since the PDFs of solar wind fluctuations in the inertial range are known to be non-Gaussian, a classical power spectrum (based on the 2^{nd} moment of the PDF) is not sufficient to completely describe the statistics of the fluctuations. In fact, the most complete information is provided by the PDF or, equivalently, by its full sets of moments $\langle \delta\phi^p \rangle$ ($p = 1, 2,\ldots$). The absolute moments of the PDF are known as structure functions. For any dynamical variable $\phi(t)$, the p^{th} *order structure function*, S_ϕ^p, is defined as:

$$S_\phi^p(\tau) = \langle |\phi(t+\tau) - \phi(t)|^p \rangle. \tag{14}$$

The variation of S with τ gives information on the scaling behavior of the data set. In the inertial range, it is shown that S takes the form of a power law of $\tau \propto \ell$:

$$S_\phi^p(\tau) = \left\langle \delta\phi_\tau^p \right\rangle \propto \tau^{\zeta(p)}, \tag{15}$$

where $\zeta(p)$, the *scaling exponent* of the structure function, is here the fundamental parameter. If $E_f \propto f^{-\alpha}$, the spectral exponent α is related to the scaling exponent of the 2^{nd} order structure function by

$$\alpha = 1 + \zeta(2). \tag{16}$$

Generally, $\zeta(p)$ is a nonlinear function of p; as mentioned above, this is related to the fact that the local Hölder exponent is not constant, characteristic of multifractality. For a *Kolmogorov-like* scaling, $\zeta(p)$ is given by

$$\zeta(p) = \frac{p}{3} + \beta(p/3), \tag{17}$$

while for a *Kraichnan-like* scaling, $\zeta(p)$ is given by Carbone (1993),

$$\zeta(p) = \frac{p}{4} + \gamma(p/4). \tag{18}$$

$\beta(p/3)$ and $\gamma(p/4)$ describe the deviations from self-similarity or scale invariance. In the absence of intermittency, $\beta = \gamma = 0$ and a linear scaling exponent, $\zeta(p) = pH$, is recovered (signature of monofractals, see Section 1).

Many models, generalizing both K41 and IK by taking into account the effects of intermittency, have been proposed to predict the variation of β and γ with p (see Marsch & Tu 1997; Horbury & Balogh 1997; Bruno & Carbone 2005, for a review). The influence of intermittency on the scaling of solar wind fluctuations has then been evaluated by using those models (Carbone et al. 1995a, 1995b; Marsch & Tu 1997, and references therein). However, these models are concerned only with a statistical and global analysis of the regularity of the turbulent fields. In order to get a local description of the degree of singularity of these fields, it is convenient to turn to methods based on wavelets.

In our present study (described in the following section), we make use of the Haar Wavelet, a square function defined between 0 and 1 and varying between −1 and 1 (Mahrt 1991) that has a very good time resolution, but a poor frequency resolution. While the use of this wavelet is not convenient in situations where narrow spectral peaks are the objects of the investigation, it seems to be well suited to the study of solar wind turbulence, characterized by featureless average power spectra, and strongly intermittent behavior, similar to what is observed in strongly turbulent neutral flows, where the fluid velocity components measured at a given point look like a usual random signal but with intermittent bursts of strong variations (e.g., Sreenivasan & Antonia 1997).

3. DATA AND WAVELET ANALYSIS TECHNIQUE

We describe here the *Wind* instrumentation and data sets used in the present study. We also provide a very simple description of the Haar Wavelet transform and the underlying technique that we apply to the *Wind* data sets.

3.1. The Data Sets

The *Wind* spacecraft, launched on 1994 November 1, was mainly designed to observe and measure the solar wind approaching Earth from a position near the Lagrange point L1. *Wind* has made a series of Earth orbits as staging to its nominal position at the L1 equilibrium point upstream, and spent extended time intervals there allowing comprehensive studies of the ambient solar wind.

For the present study, we consider data from the first *Wind* apogee pass near L1, in 1995, where the spacecraft spent several months following a series of phasing orbits. The chosen time interval is close to the previous minimum of solar activity, when well-defined periods of successive slow and fast flows can be identified. It extends from 1995 May 23rd to July 23rd. This interval was selected because no transient magnetic cloud or strong interplanetary shock was observed during these 62 days (Sanderson et al. 1998), so the analyzed properties are those of the ambient solar wind, without distinction between slow and fast streams. As a result, the structure functions that we calculate may contain a statistical mix of slow and fast wind properties, including the rapidly changing boundaries between slow and fast wind, interplanetary shocks etc. However, our conditioning technique (see Section 3.5 below) will allow to systematically eliminate those strong (non-intermittent) transient events.

We use spin resolution (3 s) magnetic field and plasma data, respectively from the Magnetic Field Investigation (MFI) experiment (Lepping et al. 1995) and the Three-Dimensional Plasma and energetic particle (3DP) experiment (Lin et al. 1995) experiment on board *Wind*. We also use accurate measurements of electron density obtained from the WAVES experiment (Bougeret et al. 1995).

MFI is a dual triaxial fluxgate magnetometer. The instrument has a variable resolution depending upon the range of operation. We use here the three components of the magnetic field vector, B_x, B_y, and Bz (in the Geocentric Solar Ecliptic (GSE) coordinate system) as well as the total magnetic field strength B with a 3 s time resolution.

The instruments on the 3DP experiment make continuous measurements of ion and electron moments at a 3 s time resolution. We mainly make use of the three components of the solar wind (proton) velocity V_x, V_y, and V_z (in the GSE

coordinate system), as well as the total proton temperature T_p and the total electron temperature T_e.

The electron density N_e is obtained from the Thermal Noise Receiver (TNR), a radio wave receiver part of the WAVES experiment. The TNR is a very sensitive digital spectrum analyzer designed to do thermal noise spectroscopy in the ambient solar wind plasma (Meyer-Vernet & Perche 1989; Issautier et al. 1999). TNR consists of several separate receivers that measure and digitize into different frequency bands between 4 kHz and 256 kHz. The electron density is determined accurately every 4.5 s from the spectrum of the quasi-thermal noise around the electron plasma frequency and it is quite immune to the spacecraft charging effects (Salem et al. 2001).

The 3DP plasma and the TNR electron density are resampled onto the time lags of the magnetic field data by linear interpolation. Also, a simple linear interpolation was used when a very few data gaps occurred.

It is worth emphasizing that simultaneous 3 s resolution magnetic field and plasma data greatly extend our study of intermittent structures to smaller scales toward the high-frequency end of the inertial range of solar wind MHD turbulence.

3.2. Wavelets in Turbulence

Ordinary Fourier techniques are commonly used in the analysis of time series. But they are inefficient in dealing with local behavior and it is clear that this inefficiency is due entirely to the nonlocal nature of the ordinary Fourier analysis, through which we compose local variations in time by using nonlocal exponentials in reconstructing the signal.

The usual tool for analyzing the frequency content of a noisy signal whose statistics depend slowly on time is the Windowed Fourier Transform (WFT). The WFT localizes a signal simultaneously in time and frequency by "looking" at it through a window of width T that is translated in time then translated in frequency (modulated in time) the same way for all analyzed frequencies: the time resolution is T and the frequency resolution is $1/T$.

Wavelet transforms represent another compromise between frequency resolution and time resolution, which depends now on the frequency. Wavelet analysis is becoming ever more popular in laboratory (e.g., Bettega & Roman 2009) and natural plasmas (e.g., Mangeney et al. 2001; Vörös et al. 2004), as well as fusion research (e.g., van Milligen et al. 1995; Bos et al. 2008), though the methods have been known and applied in other fields (such as image processing and the monitoring of electrical power systems) for quite some time.

Unlike the traditional Fourier transforms, wavelet transforms have the capability to unfold turbulence signals into both space (or time) and scale (Mallat 1989; Farge 1992); they replace time modulation by scaling to achieve frequency localization so that each component can be studied with a resolution that matches its scale (with a narrow wavelet at high frequencies or a broad wavelet at low frequencies). They favor the time resolution at the expense of frequency resolution, in degrees depending on the particular wavelet that is used, which is a good compromise for the study of a fully incoherent but highly intermittent turbulent flow like the solar wind in the Alfvénic range. This allows to localize short-lived high-frequency phenomena, such as transients or singularities (those with the highest level of fluctuations) in a signal, and zoom in on these most intermittent intervals and study their effects on the intrinsic scaling properties of the fluctuations.

Wavelet transforms have been successfully applied to the study of turbulence in neutral fluids (Farge et al. 1990; Meneveau 1991a, 1991b; Farge 1992; Katul et al. 1994a, 1994b; Katul & Parlange 1994; Katul et al. 1998; Farge et al. 2006) and more recently to the solar wind case (Veltri & Mangeney 1999; Bruno et al. 1999a, 1999b, 1999c, 2001; Vörös et al. 2004; Salem et al. 2007; Veltri et al. 2005, 2009).

For actual turbulence measurements sampled at discrete times, the appropriate wavelets are discrete wavelet transforms, defined as follows. Let $\phi_k = \phi(t_k)$ be $N = 2^M$ measured values of a quantity ϕ ($1 \leqslant k \leqslant N$), regularly sampled at times $t_k = (k-1)\,\Delta t$ (Δt being the time resolution of the data sample). The discrete wavelet transform $WT_\phi^{(m)}(j)$ of ϕ, at a scale $\tau_m = 2^m\,\Delta t$ ($1 \leqslant m \leqslant M$) and sampled at the $N/2^m = 2^{M-m}$ times $t_{m,j} = (j-1)\,\tau_m$, is given by

$$WT_\phi^{(m)}(j) = 2^{-m/2} \sum_{k=1}^{N} \phi_k \;\; \psi\left(\frac{t_k - t_{m,j}}{\tau_m}\right), \qquad (19)$$

where $\psi(t)$ is the analyzing wavelet. Equation (19) uses a logarithmic uniform spacing for the scale discretization with increasingly coarser temporal (or spatial) resolution at larger scale (Daubechies 1988; Meyer 1989; Katul et al. 1994a). Under some conditions on the analyzing wavelet, it can be shown that Equation (19) is invertible, i.e., the knowledge of $\phi - \langle\phi\rangle$ is equivalent to the knowledge of its $N-1$ wavelet coefficients $WT_\phi^{(m)}$ (Meyer 1989; Katul et al. 1994a, 1994b), $\langle\phi_k\rangle$ being the mean value of ϕ_k over the interval $N\Delta t$. Moreover, just as for the Fourier transform, there is a Bessel–Parseval theorem (Chui 1992) stating that the variance $\sigma_\phi^2 = \langle\delta\phi^2\rangle = \langle\phi_k^2\rangle - \langle\phi_k\rangle^2$ of the signal ϕ_k over this time interval is the sum of contributions from each scale (Katul et al. 1994a; Katul & Parlange 1994),

$$\sigma_\phi^2 = \langle\delta\phi^2\rangle = \frac{1}{N}\sum_{m=1}^{M}\sum_{j=1}^{2^{M-m}} \left(WT_\phi^{(m)}(j)\right)^2. \qquad (20)$$

3.3. The Haar Wavelet Transform

The Haar Wavelet basis is specifically chosen for its differencing characteristics, since we are interested in developing explicit relations between spectra or p^{th} order structure functions and the wavelet coefficients (Mahrt 1991). It was first adopted by Katul et al. (1994a, 1994b) to study the atmospheric surface layer turbulence, and later by Veltri & Mangeney (1999) and by Salem (2000) in solar wind turbulence. Moreover, it has proven to be a powerful tool in atmospheric turbulence research (see Katul et al. 1998, and references therein).

The analysing wavelet for the Haar Wavelet transform is given by Mahrt (1991),

$$\psi(t) = \begin{cases} 1 & \text{for } 0 \leqslant t < 1/2, \\ -1 & \text{for } 1/2 \leqslant t < 1, \\ 0 & \text{elsewhere.} \end{cases} \qquad (21)$$

The corresponding wavelet transform has the highest time resolution, $2\Delta t$, at the smallest scale $m = 1$. It has an interesting alternative interpretation. Indeed, it has been shown (see Beylkin et al. 1991, 1992; Katul et al. 1994a) that for this Haar Wavelet basis, the wavelet coefficients $WT_\phi^{(m)}(j)$ and the coarse grained signal $\phi^{(m)}(j)$ (equivalent to a low-pass filtered signal) at scale m can be calculated from the signal $\phi^{(m-1)}$ at scale $m-1$ according

to a simple fast pyramidal algorithm

$$WT_{\phi}^{(m)}(j) = \frac{1}{\sqrt{2}}[\phi^{(m-1)}(2i-1) - \phi^{(m-1)}(2i)], \quad (22)$$

$$\phi^{(m)}(j) = \frac{1}{\sqrt{2}}[\phi^{(m-1)}(2i-1) + \phi^{(m-1)}(2i)], \quad (23)$$

for $m = 1$ to M and $j = 1$ to 2^{M-m} for each m, given $M = \log_2(N)$ the number of scales allowed by the number of samples N. This pyramidal algorithm yields $N-1$ wavelet coefficients

$$\frac{N}{2} + \frac{N}{2^2} + \cdots + \frac{N}{2^M} = \sum_{m=1}^{M} 2^{M-m} = N - 1, \quad (24)$$

that define the orthonormal Haar Wavelet transform for the measured data set.

We want to emphasize the fact that the coarsed grained signal in Equation (23) is not exactly an average signal at scale m. The real average value $\overline{\phi}^{(m)}(j)$ of ϕ_k over the time interval $[(j-1)\Delta t_m, j\Delta t_m]$ of length $\Delta t_m = 2^m \Delta t$ is defined by

$$\overline{\phi}^{(m)}(j) = \frac{1}{2^m} \sum_{k=2^m(j-1)+1}^{2^m j} \phi_k. \quad (25)$$

This average signal $\overline{\phi}^{(m)}(j)$ is related to the coarse grained signal $\phi^{(m)}(j)$ (Equation (23)) by

$$\overline{\phi}^{(m)}(j) = 2^{-m/2}\, \phi^{(m)}(j). \quad (26)$$

The fluctuation $\delta\phi^{(m)}(j)$ at scale m can be defined as the difference between successive average values of $\phi(j)$ at the smaller scale $m-1$

$$\delta\phi^{(m)}(j) = \overline{\phi}^{(m-1)}(2i-1) - \overline{\phi}^{(m-1)}(2i). \quad (27)$$

It can easily be shown that the fluctuations $\delta\phi^{(m)}(j)$ defined by Equation (27) are directly proportional to the wavelet coefficients of Equation (22),

$$\delta\phi^{(m)}(j) = \sqrt{2^{2-m}}\, WT_{\phi}^{(m)}(j). \quad (28)$$

It is to be noted that the algorithm requires the simultaneous calculation at each scale of the fluctuation $\delta\phi(m, j)$ and of the smoothed quantity $\overline{\phi}^{(m)}(j)$, so that the effects of the large scales contained in $\overline{\phi}^{(m)}(j)$ on the fluctuation $\delta\phi^{(m)}(j)$ can be easily studied.

3.4. Analysis of Turbulence

We describe here the relations between the Haar Wavelet coefficients and the statistical quantities needed in the characterization of turbulence. The primary tool for this purpose is of course the power spectral density $E(f)$, but also the structure functions (discussed in Section 2.2) and Flatness factor, commonly used to characterize non-Gaussian fluctuations.

To determine an expression for the wavelet spectrum, we make use of the Parseval identity—Equation (20),

$$\sigma_{\phi}^2 = \sum_{m=1}^{M} \Delta f_m\; E_{\phi}(f_m), \quad (29)$$

where $f_m = 1/\tau_m = 2^{-m}/\Delta t$. Noting that $\Delta f_m / f_m = \ln(2)$, it can be easily shown that

$$E_{\phi}(f_m) = \frac{\Delta t}{\ln(2)} \left\langle \left(WT_{\phi}^{(m)}(j)\right)^2 \right\rangle, \quad (30)$$

where $\langle\cdot\rangle$ is an average in time (or in space) over all values of (j) for scale index m (see Meneveau 1991a; Yamada & Ohkitani 1990). Equation (30) shows that the wavelet power spectrum at frequency f_m is directly proportional to the average of the squared wavelet coefficients at that scale m. Because of this particular characteristics of the wavelet power spectrum, we expect it to be much smoother than its Fourier counterpart, for which the variance increases as the frequency increases and tends toward the Nyquist frequency of the measure signal (e.g., Jenkins & Watts 1968).

The wavelet coefficients can also be used to determine for any flow variable ϕ a set of functions, which are not strictly structure functions as they are usually defined (see Equation (14)), but have the same physical meaning (Mahrt 1991; Katul et al. 1994a). As shown above (see Equations (22) and (28)), the Haar wavelet coefficients are expressed as a "fluctuation" of any given variable, thus, they can be related to the p^{th}-order structure function using

$$S_{\phi}^{p}(\tau_m) = \langle |\phi(t+\tau_m) - \phi(t)|^p \rangle \sim \frac{\left\langle \left| WT_{\phi}^{(m)}(j) \right|^p \right\rangle}{2^{(\frac{m}{2}-1)\,p}}, \quad (31)$$

where the separation distance is the scale $\tau_m = 2^m \Delta t$ and the position or time is $t = (2^m j)\Delta t$. Note that the definition above (Equation (31)) of the structure functions refers only to quantities defined at scale m while their conventional definition (Equation (14)) still contains information about scales which are finer/smaller than m. One may think of the Haar Wavelet transform at scale m as an average over an interval $2^m \Delta t$ of the function $\delta\phi_m = \delta\phi(\tau_m) = \phi(t+\tau_m) - \phi(t)$, an average that diminishes "leakage" from smaller scales. Variances and higher order moments of these two differences (the one corresponding to the usual structure function definition and the one derived above in the Haar Wavelet formalism) at a given scale will be different, since in general $\langle x^p \rangle \neq \langle \overline{x}^p \rangle$, for any given random variable x, whose average over part or over the whole sample are denoted by $\overline{x}$ and $\langle x \rangle$, respectively. However, in practice the difference between both definitions of structure functions are unimportant. As discussed in the introduction (see Equation (2)), structure functions calculated using Equation (31) will have the same scaling laws as the actual structure functions (Meyer 1998). Thus in what follows, we refer to them as structure functions, without any further specification.

Naturally, the wavelet power spectrum can be expressed as a function of the second order structure function

$$E_{\phi}(f_m) = \frac{1}{4\,\ln 2}\; \frac{S_{\phi}^2(f_m)}{f_m}. \quad (32)$$

Finally, two other useful statistical measures can be defined using the wavelet coefficients as well. The wavelet skewness (SK) and the wavelet flatness (FF) at scale m, often used to characterize the intermittency of a statistically homogeneous signal (e.g., Frisch 1995), are given by

$$SK(\tau_m) = \frac{S_{\phi}^3(\tau_m)}{\left(S_{\phi}^2(\tau_m)\right)^{3/2}} = \frac{\left\langle \left(WT_{\phi}^{(m)}(j)\right)^3 \right\rangle}{\left\langle \left(WT_{\phi}^{(m)}(j)\right)^2 \right\rangle^{3/2}}, \quad (33)$$

$$FF(\tau_m) = \frac{S_\phi^4(\tau_m)}{\left(S_\phi^2(\tau_m)\right)^2} = \frac{\left\langle \left(WT_\phi^{(m)}(j)\right)^4 \right\rangle}{\left\langle \left(WT_\phi^{(m)}(j)\right)^2 \right\rangle^2}. \quad (34)$$

The Flatness is a parameter that Bruno et al. (2003) analyzed in detail using *Helios 2* data in the solar wind from 0.3 to 1 AU.

3.5. The Conditioning Scheme: Quantifying the Role of Intermittency

In fully developed neutral fluid turbulence, some local spatio-temporal order is observed, intermittently, in the form of highly coherent structures, i.e., localized regions of strong vorticity, shaped in sheets or tubes (e.g., Jimenez et al. 1993; Camussi & Guj 1997; Chainais et al. 1999, and references therein). There is now a general agreement on the existence and importance of coherent structures in fully developed turbulence (Jimenez et al. 1993), and it is expected that these small-scale structures are related to universal properties of turbulence, thereby exhibiting a generic geometric signature that may be characteristic of the cascade dynamics.

Despite several (essentially numerical) analyses (see Jimenez et al. 1993, and references therein), the role and actual shape of such structures in real turbulent flows is not fully understood. In particular, it is not well established that the flow singularities, i.e., the bursts of strong fluctuations that are responsible for intermittency, are actually coherent structures passing by the measuring instrument. Connecting the two approaches to intermittency, i.e., either from the geometry of the coherent structures, or from the statistics of turbulent fluctuations at different scales is a difficult task (see Moisy & Jiménez 2004), since statistical quantities may depend both on the geometry of the individual structures and on their spatial distribution at larger scales.

Also, there is no agreement about what method is the best to extract coherent structures from a given turbulent flow; however, the spatial information preserved by the wavelet coefficients make them well suited for identifying and extracting coherent structures (e.g., Farge 1992; Veltri 1999; Veltri & Mangeney 1999; Bruno et al. 1999a, 1999c, 2001; Salem 2000; Salem et al. 2007; Veltri et al. 2005, 2009). These structures, being localized, compress well into a wavelet basis, and are represented by a small number of large amplitude wavelet coefficients $WT_\phi^{(m)}(j)$ at a given scale m. In contrast, the remaining incoherent field, which may be thought of as background noise, will have coefficients widely spread in time and scale, with a much lower amplitude than the "coherent" coefficients. More precisely, coefficients of modulus larger than a threshold η are expected to correspond to the coherent component and the coefficients of smaller modulus will correspond to the incoherent component. Therefore, one can split the set of coefficients into two independent classes using an orthogonal wavelet transform, then reconstruct two filtered contributions that are orthogonal. Thus, the total (i.e., the original measured) field $\phi(t)$ is the sum of the coherent and the incoherent fields i.e., $\phi(t) = \phi_C(t) + \phi_I(t)$.

The value of the threshold η should ideally be taken as to ensure a vanishing probability that the wavelet coefficient of the noise will have a value larger than the threshold; however this critical threshold level will depend upon the noise, which is unknown a priori in a fully turbulent flow. There are several ways to overcome these difficulties. The first one, used for example by Farge (1992), is to proceed iteratively: choose an initial threshold, determine the resulting probability distribution of the noise coefficients, to determine a better threshold, and repeat the process. In the same spirit, Kiyani et al. (2006), in order to detect spurious multiscaling, decreased the threshold level until a mono scaling was recovered. Another, more primitive way is to choose arbitrarily the threshold, but study how results depend on this particular choice. We have chosen this last method (Veltri & Mangeney 1999; Salem 2000; Mangeney et al. 2001; Veltri et al. 2005), and defined a scale-dependent threshold η_m,

$$\eta_m^2 = F\left\langle \left|WT_\phi^{(m)}(j)\right|^2 \right\rangle = F\sigma_m^2, \quad (35)$$

$\sigma_m^2 = \langle |WT_\phi^{(m)}(j)|^2 \rangle$ being the variance at a scale m calculated over all points $j \in [1, N/2^m]$. The conditioning factor F is a constant, independent of scale, arbitrarily but meaningfully chosen so that not too many points are excluded by the conditioning (see next Section). As emphasized by Kiyani et al. (2006), such a conditioning preserves eventual scaling properties. Thus, the background component is characterized by

$$\left|WT_\phi^{(m)}(j)\right|^2 < \eta_m^2, \quad (36)$$

and the coherent component by

$$\left|WT_\phi^{(m)}(j)\right|^2 \geqslant \eta_m^2. \quad (37)$$

Once the flow has been split into a coherent component and a background incoherent component, one may calculate separately conditioned structure functions, for the total flow, the coherent component, and the background component. This technique was applied by Katul et al. (1994a, 1994b) in a study of atmospheric turbulence, and by Chainais et al. (1999) for turbulence produced in a layer between counter rotating cylinders. Note that Chainais et al. (1999) used a conditioning criterion on the pressure, which in the context of their experiment is a sensitive indicator of vortical structures.

Both Chapman et al. (2005) and Kiyani et al. (2006) also used a conditioning technique, but directly on the linear increments, in the general context of the study of biases introduced by the finite length of observational time series (see discussion in Section 7). Solar wind studies along the same lines have been published by Veltri (1999), Veltri & Mangeney (1999), Salem (2000), Bruno et al. (1999a, 1999c, 2001), Salem et al. (2007), Kiyani et al. (2006), Hnat et al. (2007), and Veltri et al. (2005, 2009). As we will see later, some of the conclusions of our work are rather insensitive to the details of the conditioning technique.

It is worth mentioning that the conditioning technique used in this paper could be, and has been, used with any of a large class of mother wavelets and relies basically on the scaling property (Equation (2)).

4. RESULTS: SPECTRA AND STRUCTURE FUNCTIONS

The above described technique is applied to our *Wind* data set described in Section 3.1. Basically, $N = 2^{21}$ data points (thus sampling $M = 21$ scales simultaneously) in the ambient solar wind in 1995 at solar minimum were used, which allows both a very good characterization of the inertial range of solar wind turbulence (Salem et al. 2007) and a sufficiently accurate determination of structure functions up to $p \leqslant 7$ or so (Anselmet et al. 1984; Marsch & Tu 1997). Spectra and structure functions are calculated for every solar wind variable considered, namely, the three components of the magnetic field B_x, B_y, B_z and the three components of the solar wind proton velocity V_x, V_y, and V_z (in the GSE coordinate system), the magnetic field strength

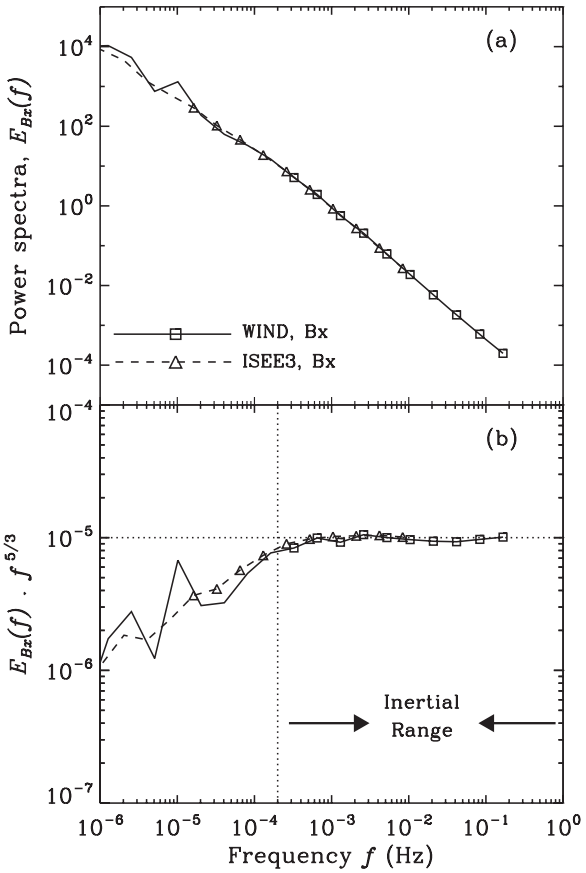

Figure 1. From top to bottom: (a) conditioned power spectra, with F = 10, for the *Wind* (solid line and squares) and for the *ISEE 3* (dashed line and triangles) X_{GSE} component of the magnetic field. The squares and triangles represent 10 scales ($m = 1$ to 10, $m = 1$ being the smallest scale) or frequencies $f_m = 2^{-m}/\Delta t$, Δt being the time resolution of the data, 3 s for *Wind* and 1 minute for *ISEE 3*, respectively. (b) Same power spectra as in (a), normalized to the Kolmogorov power law $f^{-5/3}$.

$|B|$, the magnetic energy B^2, the wind speed $|V|$, and the electron density N_e. We limit ourselves to structure functions of order as high as 6 so as not to worry about convergence problems from higher-order structure functions (Anselmet et al. 1984; Dudok de Wit & Krasnoselskikh 1996). Also, the statistics over the larger scales is not so reliable, as the number of points at a given scale m, $N/2^m$ decreases as m increases; but this is not important in our study as the inertial range of solar wind turbulence is well sampled.

4.1. Defining the Inertial Range

As mentioned above, Veltri & Mangeney (1999) were the first to apply the Haar Wavelet technique on solar wind data. They used 12 months of 1 minute resolution *ISEE 3* magnetic field and solar wind velocity data, taken in 1978–79 (with $N = 2^{19}$, thus sampling 19 scales) and calculated the corresponding spectra and structure functions. We compared their power spectrum for B_x to the one obtained with our *Wind* data set. This is illustrated in Figure 1. The upper panel shows both *Wind* (solid line and squares) and *ISEE 3* (dashed line and triangles) wavelet power spectra as a function of frequency; the squares and triangles represent the actual data points. The *ISEE 3* spectrum was shifted by a constant factor, so both power spectra can be comparable. Note that the spectra shown here are conditioned power spectra using $F = 10$. Both spectra coincide really well.

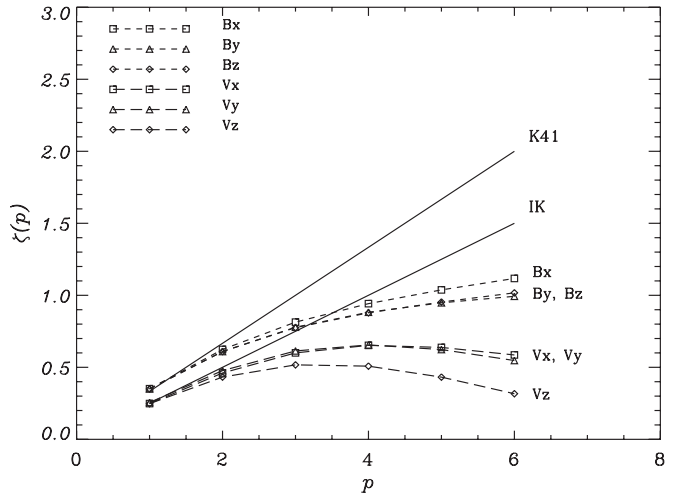

Figure 2. Scaling exponents $\zeta(p) = \zeta_p$ (Equation (15)) for the p^{th} order structure functions of the magnetic field and solar wind velocity components B_x, B_y, B_z, V_x, V_y, and V_z, as a function of p. The two solid lines represent the linear laws expected from the K41 ($\zeta_p = p/3$) and IK ($\zeta_p = p/4$) phenomenologies, Equations (17) and (18), respectively.

There appears to be a break in the spectral slope around the frequency $f \sim 10^{-4}$ Hz, above which the spectrum takes the form of a K41 power law. This is confirmed by the lower panel of Figure 1, which shows the two same spectra multiplied by $f^{5/3}$. One can immediately see that the compensated spectrum is almost flat in the range $10^{-4} < f < 10^{-1}$ Hz. Therefore, the inertial range of solar wind turbulence at 1 AU extends from frequencies of the order of 10^{-4} Hz up to the proton cyclotron frequency or so (Leamon et al. 1998, 1999; Salem 2000).

The reason why this comparison is shown here is that Veltri & Mangeney (1999) claimed they have found for the first time IK-like scaling, i.e. $f^{-3/2}$ power-law spectra, for fluctuations of all components of magnetic field and solar wind velocity except for the radial velocity V_x, which seemed curiously to have a K41 scaling. This result was inconsistent with the usual findings of K41-like scaling at least for magnetic field fluctuations in the inertial range. In their calculation of spectra and structure functions, they used 10 scales from $m = 1$ to $m = 10$; these scales correspond to a frequency range of $1.6\,10^{-5} < f < 8.3\,10^{-3}$ Hz. As seen in Figure 1, this range has a significant part outside the actual inertial range at lower frequencies and the power spectrum has two distinct slopes. This could explain why their spectral slopes, except for V_x, were actually flatter than both the K41 value 5/3 and the IK value 3/2.

In our calculation of power spectra and structure functions in the inertial range, we only consider the nine first scales from $m = 1$ to $m = 9$, corresponding to timescales of $2\,\Delta t \leqslant \tau \leqslant 2^9 \Delta t$ s or a frequency range of $6\,10^{-4} < f < 0.16$ Hz. In the following, the scaling exponents $\zeta(p)$ of structure functions (Equation (15)) are determined using a linear least squares fit on a log–log plot of structure functions versus scale or frequency.

4.2. Scaling Exponents of Structure Functions

We present here the results from our structure function analysis. Figure 2 displays the scaling exponents (Equation (15)) of the ordinary structure functions (Equation (31)) as a function of their order p for the three components of the magnetic field and solar wind velocity (Salem et al. 2007). For comparison, K41 and IK linear predictions are also shown.

We find the well-known, nonlinear, shape of $\zeta(p)$ as a function of p (Burlaga 1991; Marsch & Liu 1993; Ruzmaikin et al. 1995; Horbury et al. 1997; Horbury & Balogh 1997; Marsch & Tu 1997): intermittency severely affects the scaling exponents of all the flow variables by reducing their values from the expected K41 or IK scaling, more and more as p increases (see Section 2). The shape of these structure functions is consistent with a power-law behavior, $S^p(\tau) \sim \tau^{\zeta(p)}$, only for the lowest orders p. One can still determine the exponents $\zeta(p)$ by fitting the structure functions with power laws, although this determination becomes less and less accurate as p increases. We can already note that for the lowest orders p, the scaling exponents of the structure functions for the magnetic field and the velocity components are significantly different: the former being closer (but not equal) to a K41-scaling and the latter closer to an IK-scaling

This result is not obvious: one would expect that both dynamical variables would have a similar behavior since the inertial range is characterized by Alfvénic-type fluctuations. This shows that the nonlinear cascade may not be strongly affected by the *Alfvén effect*, contrary to the prediction by Iroshnikov (1963); Kraichnan (1965); Dobrowolny et al. (1980).

As seen in Figure 2, there is a strong deviation from Gaussianity and self-similarity (scale invariance) in the solar wind (e.g., Burlaga 1991; Marsch & Liu 1993; Veltri & Mangeney 1999; Veltri et al. 2005, 2009), even stronger than in hydrodynamic turbulence. This behavior is commonly attributed to intermittency. Is the difference of scaling between the magnetic field and velocity fluctuations also due to intermittency? This question can now be easily addressed using conditioned structure functions (defined above).

4.3. Conditioned Structure Functions and Role of Intermittency

We now refine the analysis of structure functions by adding the conditioning scheme within the Haar Wavelet technique (as defined in Section 3.5), in order to quantify the role of intermittency on the scaling properties of the fluctuations.

When the effects of the most intermittent fluctuations, above $\sqrt{F}\sigma_m$, are isolated and removed, well-defined linear scaling exponents are obtained for the fluctuations in the inertial range (Salem et al. 2007). This is illustrated in Figure 3, which displays the scaling exponents of the conditioned structure functions as a function of their order p for two different values of the conditioning factor F ($F = 5$ and $F = 20$ shown in the upper and lower panels, respectively). Compared to the nonlinear ζ_p of the ordinary structure functions (Figure 2), the scaling exponents of the conditioned structure functions are perfectly linear

$$\zeta(p) = \gamma \cdot p, \tag{38}$$

γ being a constant. The error bars in Figure 3 are very small. This is evidence of a well-defined monofractal scaling, with Hurst exponents $H = \gamma$. Surprisingly, fluctuations of all three components of the magnetic field vector display a K41-like scaling ($H \sim 1/3$), while all three components of the velocity fluctuations show an IK-like scaling ($H \sim 1/4$). Using conditioned structure functions, we have been able to clearly recover simple, monofractal scaling properties of the standard fluctuations in the inertial range, following the simple K41 and/or IK phenomenologies (Salem 2000; Mangeney et al. 2001). This shows that the multifractal nature of solar wind fluctuations is caused by the presence of intermittent structures at small scales.

What fraction of these fluctuations actually alters the monofractal behavior of turbulence in the inertial range? In other words, what value of the conditioning factor F forms a threshold above which the monofractal behavior of the scaling exponents would break. Note that the higher the conditioning factor F, the smaller the fraction of intermittent fluctuations to be removed. The answer to this question is illustrated in Figure 4. For all three components of the magnetic field and solar wind velocity fluctuations, as well as for the total fields $|B|$ and $|V|$, the magnetic energy B^2, and the electron density N_e, we calculated conditioned structure functions and their scaling exponents using values of F varying from 5 to 5000. We determined the slope γ of ζ_p for each of the above variables and each value of F considered, and, for each variable, we normalized the slope $\gamma(F)$ to $\gamma(5)$, the slope obtained for $F = 5$.

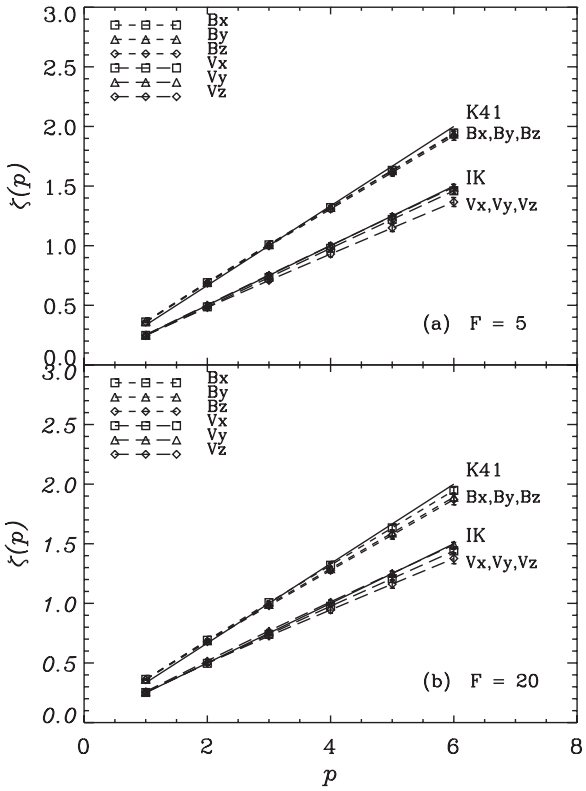

Figure 3. Scaling exponents $\zeta(p) = \zeta_p$ (Equation (15)) for the conditioned p^{th} order structure functions of the magnetic field and solar wind velocity components B_x, B_y, B_z, V_x, V_y, and V_z, as a function of p: (a) in this case, the structure functions are conditioned using $F = 5$ (see text); (b) The conditioning factor used here is $F = 20$. A higher threshold means less singular points were removed.

For the magnetic field components and strength, we find that $F \approx 20$ is a good limit value for the conditioning threshold, meaning that conditioning with any value of $F \leqslant 20$ does not change the linear relation $\zeta(p) \propto p$ and slopes of the scaling exponents shown in Figure 3. For the velocity components or $|V|$, the threshold or limit value for F is closer to 50. Indeed, for $F < 20$–50, the parameter $\gamma(F) \sim \gamma(5)$ ($\gamma(F)/\gamma(5)$ almost constant). On the contrary, the scaling exponents $\zeta(p)$ of structure functions conditioned with $F > 20$–50 start displaying a nonlinear behavior with p; the larger the F, the stronger the deviation of $\zeta(p)$ from linear behavior for the different components of the magnetic and velocity fields, but not for the density. This shows that fluctuations with amplitudes above $\sim$4 to 5σ ($\sqrt{F}\sigma$) are drastically affecting the scaling properties of all components of the magnetic and velocity fields. They are directly responsible for the multifractal behavior of magnetic field and solar wind velocity fluctuations.

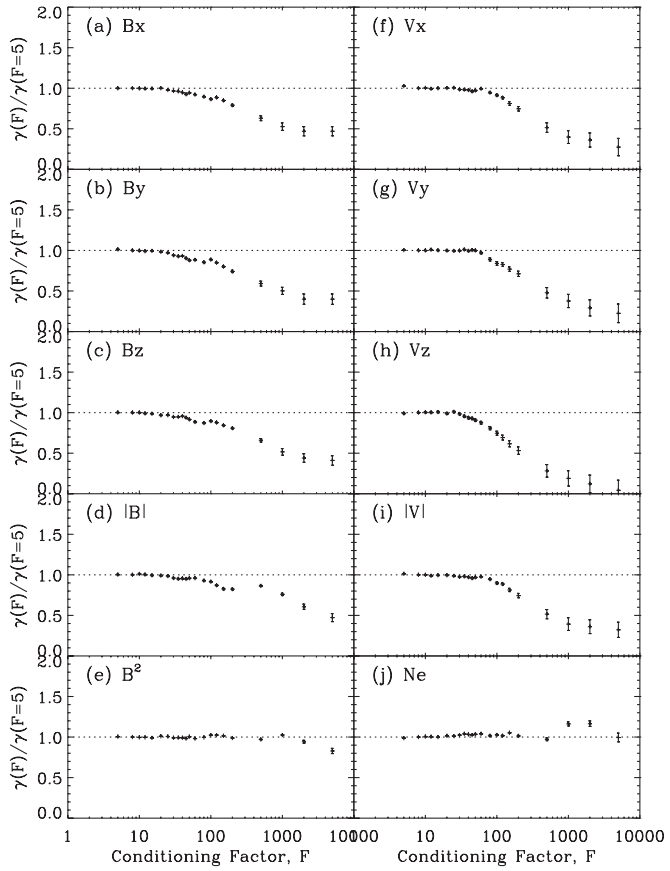

Figure 4. Slope of the scaling exponents ζ_p of the conditioned structure functions (see Figure 3) for different values of the conditioning factor F, varying from 5 to 5000, normalized to the slope for $F = 5$. Each panel from (a) to (j) represents a different variable, the magnetic field and solar wind velocity components B_x, B_y, B_z, V_x, V_y, and V_z, the magnetic field strength $|B|$, the solar wind speed $|V|$, the magnetic energy B^2, and the electron density N_e, respectively.

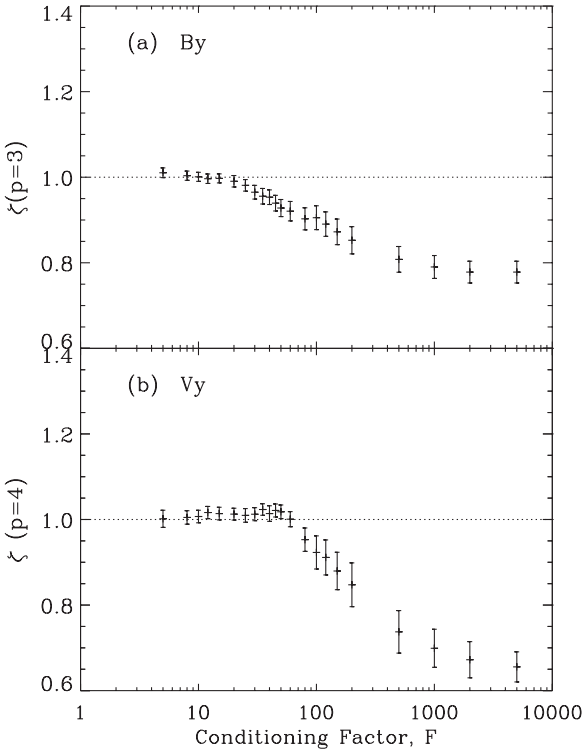

Figure 5. Panel (a) shows the value of ζ_p for $p = 3$ for the conditioned structure function of B_y as a function of the conditioning factor F; $\zeta_3 = 1$ (dotted line) is what is expected in the K41 phenomenology; Panel (b) shows the value of ζ_p for $p = 4$ for the velocity component V_y as a function of F. The dotted line indicates $\zeta_4 = 1$, value that is expected in the IK phenomenology.

Furthermore, the plasma density N_e and the magnetic energy B^2 both display a K41-like scaling in the inertial range (not shown here). The slopes of the scaling exponents of their structure functions are observed to be quite constant with F (see Figures 4(a) and (b)), up to $F \sim 1000$ above which conditioning becomes negligible (i.e., almost no conditioning is applied for such values of F). This shows that N_e and B^2 are much less intermittent than the components of the magnetic field and/or velocity vectors, in agreement with recent results obtained by Hnat et al. (2007) using a conditioning scheme similar to ours. This also means that intermittency is not completely absent for N_e and B^2, as has been shown in recent analyses that did not use any conditioning scheme(Podesta et al. 2006b; Podesta 2007; Chang et al. 2008).

To emphasize the fundamental difference in scaling for magnetic field and velocity fluctuations, and the fact that they are both extremely close (or almost equal) to the K41 and IK scaling respectively, we took a close look at the scaling exponents for the components B_y and V_y. The K41 theory predicts $\zeta_3 = \zeta(p = 3) = 1$; It's actually an exact result (Frisch 1995). The IK phenomenology predicts that $\zeta_4 = \zeta(p = 4) = 1$. Is this observed in our data set? How does this result vary with the conditioning factor F? So, we determined the values of scaling exponent for $p = 3$ for B_y and for $p = 4$ for V_y for our range of conditioning factor F. The result is shown in Figure 5. Again, one can see, indeed, that for B_y (Figure 5, upper panel), $\zeta_3 \sim 1$ for $F \leqslant 20$, and for V_y (Figure 5, the lower panel), $\zeta_4 \sim 1$ for $F \leqslant 50$.

5. SCALING OF PROBABILITY DISTRIBUTION FUNCTIONS

A different description of the same information is through the PDFs of the fluctuations. PDFs of turbulent fluctuations are recognized as an important diagnostic of fluid turbulence (Frisch 1995; Biskamp 1993, 2003). The information they contain is in principle equivalent to that contained in the whole set of structure functions, for all values of the order p. It has been shown (Burlaga 1993; Marsch & Tu 1994; Feynman & Ruzmaikin 1994; Marsch & Tu 1997; Sorriso-Valvo et al. 1999; Salem 2000; Sorriso-Valvo et al. 2001; Bruno et al. 2004) that these PDFs are approximately Gaussian for timescales longer than a few hours (for scales larger than those of the inertial range), but show strong deviations from a Gaussian PDF at smaller scales, with heavy tails and statistical properties dominated by intermittent bursts of large amplitude perturbations.

Figure 6 displays the PDF of the Haar Wavelet coefficient WT_{B_x} for the Bx component of the magnetic field for the scale $m = 1$ ($\tau = 6$ s). Note that the wavelet coefficient is directly proportional to the corresponding fluctuation, $\delta B_x(m, i) = \sqrt{2^{2-m}}\ WT_{B_x}(m, i)$ (Equation (28)). The vertical dashed lines indicate the threshold $\sqrt{F}\,\sigma_W$, for $F = 20$. Basically, the conditioning process (Equations (36) and (37)) consists of cutting the tails of the PDFs above the chosen threshold. The wavelet coefficients above the threshold represent in this case 0.4% of the data set or time series, and they characterize the most active, intermittent structures that drastically alter the linear

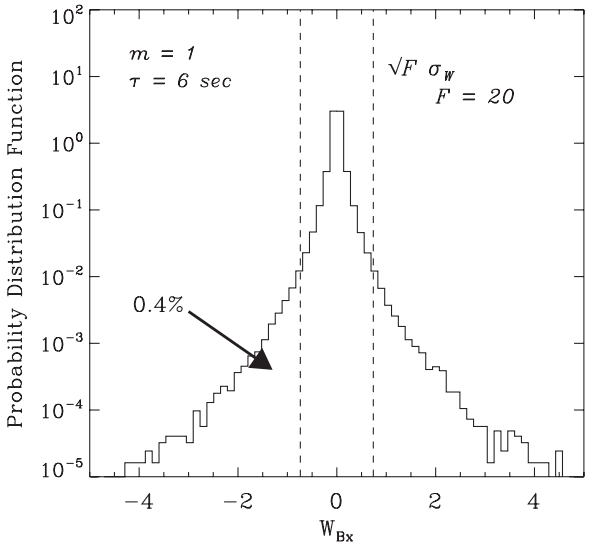

Figure 6. Probability Distribution Function (PDF) of the Haar wavelet coefficient for the component Bx at the smallest scale $m = 1$ is plotted. Note that the wavelet coefficients of a given variable are proportional to the fluctuation of that variable, according to Equation (28). The vertical dashed lines indicate the threshold $\sqrt{F}\,\sigma_W$, for $F = 20$. The wavelet coefficients above the threshold represent in this case 0.4% of the corresponding data set or time series, and they characterize the most active, intermittent structures that drastically alter the linear scaling exponents ζ_p.

scaling exponents ζ_p. Table 1 summarizes, for each variable at the smallest scale $m = 1$ (or $\tau = 6$ s), the percentage of singular points removed from the original data set for different conditioning factors F. The last column of this table gives the percentage of singular points when all variables are combined together. As shown in Table 1, the singular points responsible for the multifractal properties of the fluctuations represent a tiny fraction of the original data set: less than 1% for $F = 20$ at $m = 1$. Those percentages drop significantly for scales $m > 1$, and the larger the scale the smaller the percentages; note that in our conditioning scheme F is constant and independent of scale.

Using Equation (28), we can easily calculate the PDFs (of increments) for any variable ϕ by computing the histogram of the wavelet coefficients. It is commonly believed that PDFs of solar wind fluctuations do not rescale in the inertial (e.g., Bruno et al. 2004, 2005). However, we find that they actually rescale naturally all throughout the inertial range using a simple scaling relation, provided that a proper conditioning is applied. The self-similar scaling of those truncated PDFs is compatible with the scaling of conditioned structure functions (see below). Let $P(\delta\phi_m)$ be the PDF of a fluctuating quantity $\delta\phi_m$ at a scale m. The corresponding structure function is proportional to the moments of the PDF

$$\left\langle \delta\phi_m^p \right\rangle = \int_{-\infty}^{+\infty} d\delta\phi_m \delta\phi_m^p P(\delta\phi_m). \tag{39}$$

Now, if we assume that the PDF are self-similar and rescale in the inertial range according to

$$\delta\phi_m = 2^{\alpha_m}\delta\phi_1, \tag{40a}$$

$$P(\delta\phi_m) = 2^{\beta_m} P(\delta\phi_1), \tag{40b}$$

where are two coefficients depending on the scale m, then the structure function (Equation (39)) can be rewritten as:

$$\left\langle \delta\phi_m^p \right\rangle = 2^{\alpha_m (p+1)+\beta_m} \left\langle \delta\phi_1^p \right\rangle. \tag{41}$$

The normalization condition $\int_{-\infty}^{+\infty} P(\delta\phi_m)\, d\delta\phi_m = 1$ leads to $\alpha_m + \beta_m = 0$, so that

$$\left\langle \delta\phi_m^p \right\rangle = 2^{\alpha_m p} \left\langle \delta\phi_1^p \right\rangle. \tag{42}$$

Using Equation (15) and $\tau_m = 2^m$, we can easily show that

$$\left\langle \delta\phi_m^p \right\rangle = 2^{(m-1)\zeta(p)} \left\langle \delta\phi_1^p \right\rangle. \tag{43}$$

Therefore, by identification of Equations (42) and (43), and using $\zeta(p) = \gamma \cdot p$ ($\gamma \sim 1/3$ for the scaling of $B_{x,y,z}$ and $\gamma \sim 1/4$ for $V_{x,y,z}$, see Figure 3), we get $\alpha_m = -\beta_m = (m-1)\gamma$, and, thus, the following scaling for the PDFs throughout the inertial range

$$\delta\phi_m = 2^{\gamma(m-1)}\,\delta\phi_1, \tag{44a}$$

$$P(\delta\phi_m) = 2^{-\gamma(m-1)}\, P(\delta\phi_1). \tag{44b}$$

To illustrate the above scaling properties, we have plotted in Figure 7, the PDFs of all three components of the magnetic field fluctuations (upper three panels) and all three components of the velocity fluctuations (lower three panels), conditioned with $F = 20$, at scale $m = 1$, and overplotted the corresponding scaled PDFs for $m = 2$ to 7, using Equations (44a) and (44b) (and different colors). This demonstrates that there is indeed a self-similar structure throughout the inertial range. As discussed for instance by Bruno et al. (2005), if there is scale invariance and if we use the standardized variable $\delta\Phi_m = \delta\phi_m \big/ \left\langle \delta\phi_m^2 \right\rangle^{1/2}$ instead of $\delta\phi_m$, the PDFs of the fluctuations of $\delta\Phi_m$ should converge to the same PDF. This is completely consistent with our scaling above: if we use $\delta\Phi_m$ in the scaling above, then Equation (44a) reduces to $\delta\Phi_m = \delta\Phi_1$, and consequently $P(\delta\Phi_m) \equiv P(\delta\Phi_1)$.

Several authors (e.g. Sorriso-Valvo et al. 1999, 2001; Forman 2003; Forman & Burlaga 2003), assuming that PDFs do not rescale in the inertial range, have used the Castaing model (Castaing et al. 1990) to characterize the shape of the PDFs via the scaling laws of parameters that describe the variation of the shape of the PDFs with scale. In this model, the final PDF is the convolution of Gaussian distributions of width σ, the distribution of which is chosen to be log-normal. The impression that the PDFs do not rescale in the inertial range may be due to the fact that the largest scale of the inertial range is not always known a priori, unless one looks at power spectra at the same time to define it (see Section 4.1). For example, Sorriso-Valvo et al. (1999, 2001) fitted the Castaing model to observed PDFs at scales ranging between 81 s and 23 hr, using solar wind data at 1 AU. But the Castaing parameters of their fit exhibit a well-defined scaling only at scales smaller than 1.5 hr, which correspond to the inertial range (as discussed in Section 4.1).

Finally, it is worth emphasizing the conditioning criterion used to remove intermittency as the key feature of our wavelet technique. The conditioning scheme within the Haar Wavelet transform induces a self-similar behavior of the fluctuations, by rejecting very large amplitude singular points (above $\sqrt{F}\,\sigma_W$) from the standard fluctuations.

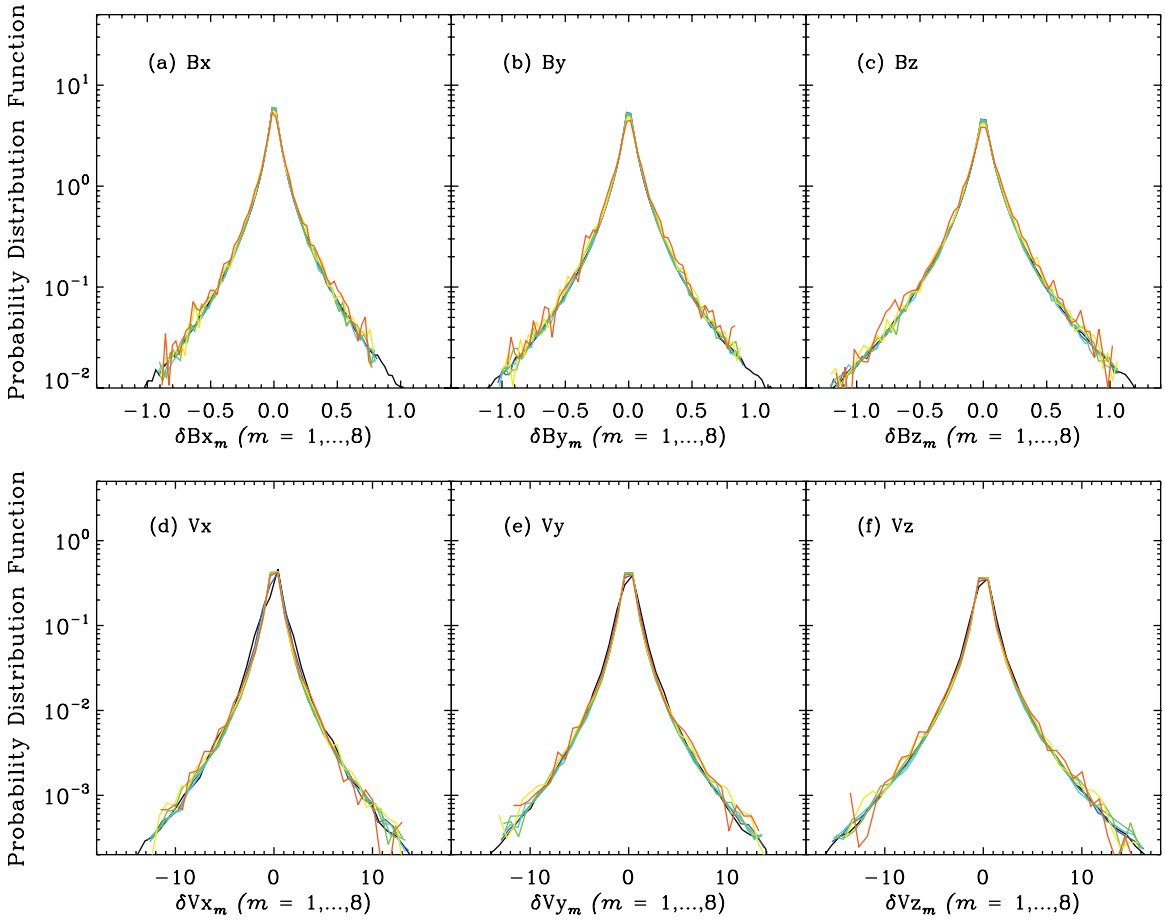

Figure 7. PDFs of the magnetic field and solar wind velocity fluctuations (Equation (28)), basically the increments of a given quantity or variable) at scales $m = 1$ to 7, conditioned with $F = 20$. The top panels show the PDFs of the magnetic field components, and the bottom panels the PDFs of the solar wind velocity components. For each variable, the PDF at scale m has been rescaled with respect to the PDF at scale $m = 1$ according to the scaling given by Equations (44a)–(44b). As a result, the conditioned PDFs fall on top of each other for each scale m throughout the inertial range: the black PDFs correspond to scale $m = 1$, dark blue to $m = 2$, light blue to $m = 3$, green to $m = 4$, light green to $m = 5$, yellow to $m = 6$ and red to $m = 7$.

(A color version of this figure is available in the online journal.)

Table 1
Percentage of Singular Points (Equation (37)) at Scale $m = 1$ for Different Values of the Conditioning Factor F, for Each Variable Individually

F	B_x	B_x	B_x	$\|B\|$	V_x	V_y	V_z	N_e	Te	T_p	All
5	1.77	1.79	1.68	1.35	1.77	1.77	1.77	1.62	1.57	1.97	9.20
10	0.86	0.87	0.83	0.69	0.77	0.82	0.85	0.72	0.58	0.84	4.58
20	0.38	0.39	0.38	0.34	0.32	0.34	0.37	0.29	0.18	0.31	2.05
50	0.11	0.12	0.12	0.12	0.08	0.09	0.11	0.08	0.03	0.08	0.63

Note. The last column gives the percentage of singular points when all variables are combined.

6. THE ALFVÉN RATIO, KINETIC TO MAGNETIC ENERGY RATIO

The Alfvén ratio (e.g. Bruno et al. 1985; Goldstein et al. 1995a) is defined as:

$$R_A(f) = \frac{E_V(f)}{E_b(f)}, \tag{45}$$

where $E_V(f)$ and $E_b(f) = E_B(f)/(4\pi\rho)$ are the power spectral density of the velocity and magnetic field fluctuations. In the IK phenomenology (Kraichnan 1965), where equipartition is reached at small scales, the Alfvén ratio should remain close to 1. However, for reasons which are still unclear, in the solar wind, the magnetic energy is observed to dominate, $R_A < 1$, at least in the low frequency part of the inertial range (Bruno et al. 1985; Goldstein et al. 1995a; Tu & Marsch 1995; Bavassano et al. 1998). Goldstein et al. (1995a), using *Helios* data, have observed a decrease of R_A with distance from the sun, from $R_A \simeq 1$ at 0.3 AU to $R_A \sim 0.5$ at 1 AU.

The Alfvén ratio for the present set of observations is shown in Figure 8. While kinetic energy dominates at the larger scale, in the inertial range R_A increases from the commonly observed value $R_A \simeq 0.5$ at 10^{-4}–10^{-3} Hz (Bruno et al. 1985; Roberts et al. 1987a, 1987b, 1990, 1992; Matthaeus & Goldstein 1982; Goldstein et al. 1997) to a near equipartition value $R_A \geqslant 1$ at smaller scale and above (see also Salem 2000; Podesta et al. 2007). However, for timescales $\tau \leqslant 30$ s, the kinetic energy seems to be dominating.

The observed values of the Alfvén ratio in the inertial range are not really understood yet. This unbalance between magnetic

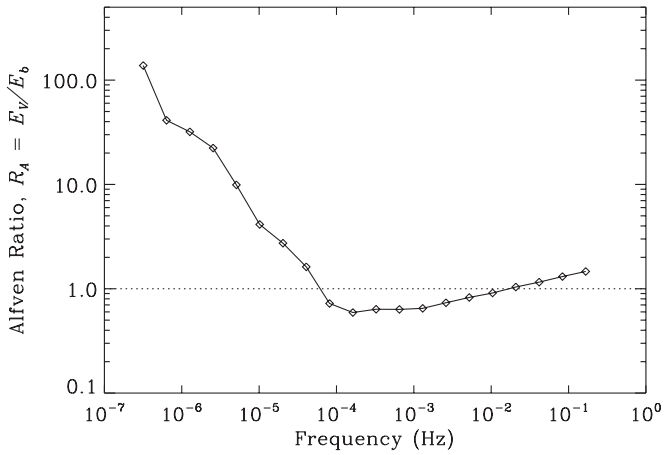

Figure 8. Alfvén ratio (kinetic to magnetic energy ratio) shown as a function of frequency. The diamonds represent the data points, corresponding to the scales sampled here.

and kinetic energy can be explained (see Grappin et al. 1991; Müller & Grappin 2004, 2005; Bruno & Carbone 2005) as a competing action between the Alfvén effect (Kraichnan 1965) leaning toward equipartition (see Section 2), and the nonlinear terms (Grappin et al. 1983). This competing action could lead to either an excess of magnetic energy or an excess of kinetic energy, as it is observed in the solar wind. In addition, recent theoretical studies seem to find a similar unbalance between magnetic and kinetic energy in the inertial range when nonlocal effects are involved, such as large and small k-coupling (Galtier 2006; Mininni et al. 2007).

Finally, given the unbalance between magnetic and kinetic energies, and the different scaling properties of the magnetic field and velocity fluctuations, would the description of MHD turbulence in terms of Elsässer variables (Elsässer 1950), $\mathbf{z}^{\pm} = \delta\mathbf{V} \pm \delta\mathbf{B}/\sqrt{4\pi\rho}$ coupling $\delta\mathbf{V}$ and $\delta\mathbf{B}$ together, even be theoretically appropriate? Figure 9 displays two-dimensional histograms of the Alfvénicity of the standard fluctuations (below 4–5 σ), i.e. the correlation between the X-GSE component of the velocity fluctuations δV_x and the same component of the magnetic field fluctuations $\delta B_x/\sqrt{4\pi\rho}$ in units of speed, at different scales of the inertial range. The different contours represent the number of occurrence. This figure shows that the correlation between $\delta\mathbf{V}$ and $\delta\mathbf{B}$ throughout the inertial range is highly variable (see Figure 9) and scattered around $\delta\mathbf{V} \pm \delta\mathbf{B}/\sqrt{4\pi\rho} = 0$ (Salem et al. 2007). Therefore, the Elsässer variables are no better of a choice than the variables $\delta\mathbf{V}$ and $\delta\mathbf{B}$ separately.

7. DISCUSSION AND CONCLUSION

In this paper, we have discussed, improved and generalized results that have been presented by Veltri (1999), Veltri & Mangeney (1999), Salem (2000), Mangeney et al. (2001), and Veltri et al. (2005), concerning the scale invariance and intermittency properties of MHD turbulence as derived from a wavelet analysis of solar wind data.

An important aspect of the present work is the use of very long samples of *Wind* 3 s resolution magnetic field and particle data, allowing to investigate simultaneously magnetic field and plasma fluctuations with the same, relatively high, time resolution.

As usual, the statistics of all these fluctuations are observed to be non-Gaussian all throughout the inertial range, and display anomalous (multifractal) scaling, when analyzing their PDFs and structure functions, respectively. However, as previously reported by Salem (2000), Mangeney et al. (2001), and Podesta et al. (2006a), we confirm that the magnetic field and plasma bulk velocity have fundamentally different scaling laws, close to K41 for the magnetic field components, and close to IK for the velocity components, a result which poses a puzzling theoretical problem in MHD turbulence. Kinetic effects are not expected to be responsible for the different scaling of magnetic and velocity fields, but the strong anisotropy of solar wind fluctuations, or the influence of compressibility may however play a role. Our conditioning scheme is presently being generalized to include the effects of the solar wind speed, compressibility, and fluctuation anisotropies in order to gain further insight on the different scaling properties of the magnetic and velocity fields in various states of the solar wind (fast and slow streams, for example).

Although the fluctuations of all usual fields display a multifractal character, we found that eliminating the most intense bursts of fluctuations by using a conditioning scheme, allows to recover a monofractal behavior. The PDFs still remain non-Gaussian, but the conditioning removes the "fat tails" for the highest amplitudes; the resulting truncated PDFs rescale perfectly at all scales in the inertial range, while the conditioned scaling exponents follow a linear law, with a Hurst exponent $H \sim 1/3$ (similar to K41) for the magnetic field components and $H \sim 1/4$ (close to IK) for the velocity components.

Basically, the use of the conditioning scheme reveals the self-similar behavior of the fluctuations. Such a behavior under conditioning has been observed in several instances. For example, Katul et al. (1994a), studying atmospheric surface layer turbulence, noticed that eliminating events beyond a certain threshold in the inertial subrange also eliminated the multiscaling characteristic of intermittency. Similarly, Chainais et al. (1999), considering turbulence in a swirling flow, could define, by using a suitable conditioning criterion, what they call a background flow characterized by a monofractal structure.

Studies of the quantities δn_p, $\delta(B^2)$, and $\delta(n_p V^2)$ in the solar wind have shown that they display some intermittent behavior (Hnat et al. 2002; Kiyani et al. 2006; Hnat et al. 2007; Podesta 2007; Chang et al. 2008). Furthermore, using a conditioning technique similar to ours, Kiyani et al. (2006) and Hnat et al. (2007) have shown that, after removing a small but sufficient number of particularly "singular" points in the time series, the fluctuations took a monofractal character, with a relatively well defined Hurst exponent. They concluded that the multifractality observed without conditioning was probably an artifact, "spurious multi-affinity" (Chechkin & Gonchar 2000), due to the finite length of the time series, which affects the statistics of extreme events (see also Dudok de Wit & Krasnoselskikh 1996; Kiyani et al. 2009). This is actually a particular case of phenomenon, known as "linearization," which can be given a simple although not mathematically rigorous explanation (see Abry et al. 2007).

This linearization is due to the fact that the PDF of the fluctuations are heavy tailed, with a small but finite probability of having a very large fluctuation combined with a finite sample size of the time series. This means that the tails are poorly sampled statistically, so that the large fluctuations may be present or not in the observed time series. The impact on the high order statistical moments of the PDFs may be considerable.

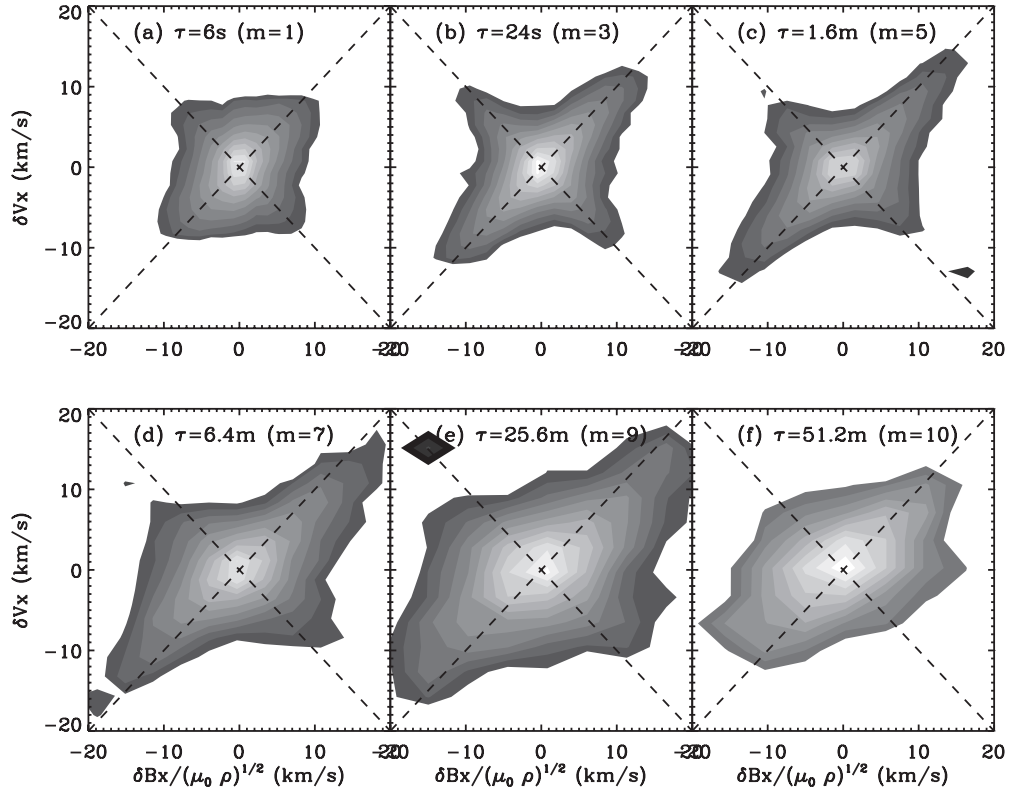

Figure 9. Two-dimensional histograms of the Alfvénicity of the fluctuations below 4–5 σ (conditioned with $F = 20$) at different scales throughout the inertial range. The different panels show the velocity fluctuations versus the magnetic fluctuations (in the X-GSE direction) in the same units (of speed) at different scales from $m = 1$ (panel a) to $m = 10$ (panel f). The dashed lines indicate $\delta V_i = \pm \delta B_i / \sqrt{\mu_0 \rho}$, lines where the Alfvénicity is maximum and equal to ± 1.

To illustrate that point, let us return to the definition of the average structure function $S_\phi^p(\tau_m)$ of order p (Equation (31)), where the separation distance is the scale $\tau_m = 2^m \Delta t$, and the average is taken over the $N_m = N/2^m = 2^{M-m}$ times $t_j = (2^m j)\,\Delta t$, with $j \in [1, N_m]$. The scaling exponents $\zeta(p)$ are calculated via a linear regression of the logarithm of the structure function over a limited range of scales τ_m, $m \leqslant m_\star \leqslant M$, so that in what follows $\sum$ stands for $\sum_{m=1}^{m_\star}$. This results in the estimate of $\hat{\zeta}(p)$ which can be expressed as:

$$\hat{\zeta}(q) = \sum w_m \log_2 S_\phi^p(\tau_m), \tag{46}$$

the weigths w_m satisfying $\sum w_m = 0$ and $\sum m\, w_m = 1$.

For large values of p, the structure functions $S_\phi^p(\tau_m)$ are driven by the largest fluctuations $\left|WT_\phi^{(m)}(j)\right|^p$ at scale m, obtained from the N_m samples of the time series,

$$W_{\max}^{(m)} = \max_j \left[\frac{\left|WT_\phi^{(m)}(j)\right|}{2^{(\frac{m}{2}-1)}} \right], \tag{47}$$

i.e. for large p,

$$S_\phi^p(\tau_m) \sim \frac{1}{N_m} \left(W_{\max}^{(m)}\right)^p,$$

and

$$\log_2 S_\phi^p(\tau_m) \sim -\log_2 N_m + p \log_2 W_{\max}^{(m)}. \tag{48}$$

Note that the definition of N_m implies that $\sum w_m \log_2 N_m = 1$. The statistical properties of extreme values of the fluctuations of multifractal processes, in the heavy tails of their PDF, are not known theoretically, but various numerical simulations are more or less consistent with a power law

$$W_{\max}^{(m)} \sim c_N \tau_m^{h_c}. \tag{49}$$

For a multifractal, the exponent h_c may be interpreted as the smallest local Hölder exponent for the N_m samples of the times series. Indeed the multifractal analysis associates to each time position t_j a Hölder exponent such that $\left|WT_\phi^{(m)}(j)\right| \sim c_j \tau_m^{h(t)}$, the largest increments being obtained for the smallest h, where ϕ is the most singular. Then, as $p \to \infty$,

$$\hat{\zeta}(p) \sim \sum w_j (\log_2 N_m + p h_c j + \text{cste}) = 1 + p h_c, \tag{50}$$

meaning that the scaling exponent $\hat{\zeta}(p)$ becomes a linear function of p. On the other hand, for small values of p, the estimation of the scaling exponent becomes close to the actual exponent, $\hat{\zeta}(p) = \zeta(p)$. Thus, for a monofractal with a Hurst exponent H, the estimated scaling exponent is expected to follow a linear relation with a slope H for small values of p and another linear relation with a new slope h_c for large values of p.

Extreme events are therefore particularly relevant to the description of the scaling properties of random phenomena, involving a heavy tailed PDF that decreases slowly and roughly follows a power law. As discussed by Muzy et al. (2006), the observed extreme value statistics result from a competition between an increase of the number of independent samples (which tends to increase typical extreme values) and a decrease of the sampling scale (which tends to decrease typical observed values). It is also clear that conditioning with an increasing threshold (i.e., fewer and fewer intermittent structures to be

removed) will tend to diminish the tendency toward linearization of the scaling exponents, as demonstrated by Kiyani et al. (2006).

Thus we are faced with the question: is MHD turbulence in the solar wind actually monofractal, the finite size of the time series producing a "spurious multi-affinity," or does a proper conditioning allow to separate efficiently the fluctuations into a monofractal "background" and localized, intermittent, coherent structures. The answer is not an easy one; one may think of two ways to obtain an answer.

The first one is to study the local regularity of the fluctuations, instead of limiting oneself to a study of the statistical description of this regularity as done when using the multifractal formalism; those two approaches should then give the same statical results. However, such a study is a difficult one, as discussed for example by Katul et al. (2001). However, new methods have been developed (see, e.g., Turiel et al. 2008, and references therein), which could be applied in the solar wind context. Furthermore, since the conditioning appears to produce the same results in widely different situations, it would be interesting to apply it to some artificial time series whose properties are well known.

The second approach aims at studying the coherent structures, i.e., the extreme events. The thresholding technique used here, based on a simple classification of the wavelet coefficients, allows for a direct and systematic identification of the most active, singular structures responsible for the intermittency in the solar wind. A close look at the data shows that the intermittent or singular fluctuations are very localized in time and scale. Using 1 minute resolution *ISEE 3* magnetic field and plasma data, Veltri & Mangeney (1999) were able to show for the first time that the most intermittent fluctuations were coherent structures, represented by one-dimensional current sheets and shock waves (Veltri et al. 2005, 2009). The higher time resolution of our *Wind* data sets reveal new structures at smaller scales, some of which are identified as magnetic holes, small-scale magnetic flux tubes and soliton-like Alfvènic perturbations, for the first time directly detected in the data. The physical nature and properties of these intermittent structure will be presented in a forthcoming paper.

In parallel, different techniques to detect coherent structures in turbulent signals are being developed. The first one is a new technique by Li (2008) aimed to detect current sheet-like structures in the solar wind. The second one is a new method by Sahraoui (2008) based on the use of the Fourier phases to detect coherent structures in turbulent time series and to relate them to intermittency. The emergence of such powerful techniques will allow for a full investigation of the physical nature and properties of intermittent structures in the turbulent solar wind. This is important for a good understanding of how these structures form and where they originate from. Whether these coherent structures originate at the Sun or are locally generated by turbulence dynamics still remains an open question.

C.S. thanks Dr. R. Bruno, Prof. G. Li, and Dr. F. Sahraoui for useful discussions on this work, and A. Coddington for his valuable editorial suggestions. Work at UC Berkeley was supported by NASA grant numbers NNG04GG08G and NNX07AD91G.

REFERENCES

Abry, P., Pipiras, V., & Wendt, H. 2007, in Proc. 21st GRETSI Symposium on Signal and Image Processing (Troyes: GRETSI), 433
Anselmet, F., Gagne, Y., Hopfinger, E. J., & Antonia, R. A. 1984, J. Fluid Mech., 140, 63
Arneodo, A., Argoul, F., Bacry, E., Elezgaray, J., & Muzy, J. F. 1995, Ondelettes, Multifractakes et Turbulences: de l'ADN aux croissances cristallines (Diderot Editeur, Art et Sciences, Paris, France)
Arneodo, A., Grasseau, G., & Holschneider, M. 1988, Phys. Rev. Lett., 61, 2281
Bacry, E., Arneodo, A., Frisch, U., Gagne, Y., & Hopfinger, E. 1991, in Turbulence and Coherent Structures, Proc. Turbulence 89 Conf., ed. O. Metais & M. Lesieur (Dordrecht: Kluwer), 203
Bacry, E., Muzy, J. F., & Arnéodo, A. 1993, J. Stat. Phys., 70, 635
Bale, S. D., Kellogg, P. J., Mozer, F. S., Horbury, T. S., & Reme, H. 2005, Phys. Rev. Lett., 94, 215002
Bavassano, B., Pietropaolo, E., & Bruno, R. 1998, J. Geophys. Res., 103, 6521
Bettega, G., & Roman, H. E. 2009, Europhys. Lett., 85, 35001
Beylkin, G., Coifman, R., & Rokhlin, V. 1991, Commun. Pure Appl. Math., 44, 141
Beylkin, G., Coifman, R., & Rokhlin, V. 1992, in Wavelets and their Applications, ed. M. B. Ruskai, G. Beylkin, & R. Coifman (Jones and Bartlett Books in Mathematics; Boston, MA: Jones and Bartlett Publishers), 474
Biskamp, D. 1993, Nonlinear Magnetohydrodynamics, Cambridge Monographs on Plasma Physics (New York, NY: Cambridge Univ. Press)
Biskamp, D. 2003, Magnetohydrodynamic Turbulence (Cambridge: Cambridge Univ. Press), 310, ISBN 0521810116
Bos, W. J. T., Futatani, S., Benkadda, S., Farge, M., & Schneider, K. 2008, Phys. Plasmas, 15, 072305
Bougeret, J.-L., et al. 1995, Space Sci. Rev., 71, 231
Bruno, R. 1997, Nuovo Cimento C, 20, 881
Bruno, R., Bavassano, B., Bianchini, L., Pietropaolo, E., Villante, U., Carbone, V., & Veltri, P. 1999a, in ESA Special Publication, Vol. 448, Magnetic Fields and Solar Processes, ed. A. Wilson (Noordwijk: ESA), 1147
Bruno, R., Bavassano, B., Pietropaolo, E., & Carbone, V. 1999b, in AIP Conf. Ser., Vol. 471, Solar Wind Nine, ed. S. R. Habbal, R. Esser, J. V. Hollweg, & P. A. Isenberg (Melville, NY: AIP), 539
Bruno, R., Bavassano, B., Pietropaolo, E., Carbone, V., & Veltri, P. 1999c, Geophys. Res. Lett., 26, 3185
Bruno, R., Bavassano, B., & Villante, U. 1985, J. Geophys. Res., 90, 4373
Bruno, R., & Carbone, V. 2005, Living Rev. Solar Phys., 2, 4
Bruno, R., Carbone, V., Bavassano, B., & Sorriso-Valvo, L. 2005, Adv. Space Res., 35, 939
Bruno, R., Carbone, V., Chapman, S., Hnat, B., Noullez, A., & Sorriso-Valvo, L. 2007a, Phys. Plasmas, 14, 032901
Bruno, R., Carbone, V., Primavera, L., Malara, F., Sorriso-Valvo, L., Bavassano, B., & Veltri, P. 2004, Ann. Geophys., 22, 3751
Bruno, R., Carbone, V., Sorriso-Valvo, L., & Bavassano, B. 2003, J. Geophys. Res. (Space Phys.), 108, 1130
Bruno, R., Carbone, V., Veltri, P., Pietropaolo, E., & Bavassano, B. 2001, Planet. Space Sci., 49, 1201
Bruno, R., D'Amicis, R., Bavassano, B., Carbone, V., & Sorriso-Valvo, L. 2007b, Ann. Geophys., 25, 1913
Burlaga, L. F. 1991, J. Geophys. Res., 96, 5847
Burlaga, L. F. 1993, J. Geophys. Res., 98, 17467
Camussi, R., & Guj, G. 1997, J. Fluid Mech., 348, 177
Carbone, V. 1993, Phys. Rev. Lett., 71, 1546
Carbone, V., Bruno, R., Sorriso-Valvo, L., & Lepreti, F. 2004, Planet. Space Sci., 52, 953
Carbone, V., Bruno, R., & Veltri, P. 1995a, in Lecture Notes in Physics, Vol. 462, Small-scale Structures in Three-dimensional Hydrodynamic and Magnetohydrodynamic Turbulence, ed. M. Meneguzzi, A. Pouquet, & P.-L. Sulem (Berlin: Springer), 153
Carbone, V., Bruno, R., & Veltri, P. 1996a, Geophys. Res. Lett., 23, 121
Carbone, V., Veltri, P., & Bruno, R. 1995b, Phys. Rev. Lett., 75, 3110
Carbone, V., Veltri, P., & Bruno, R. 1996b, Nonlinear Process. Geophys., 3, 247
Castaing, B., Gagne, Y., & Hopfinger, E. J. 1990, Physica D: Nonlinear Phenomena, 46, 177
Chainais, P., Abry, P., & Pinton, J.-F. 1999, Phys. Fluids, 11, 3524
Chang, T., Cheng-Chin, W., & Podesta, J. 2008, in AIP Conf. Ser., Vol. 1039, Particle Acceleration and Transport in the Heliosphere and Beyond, ed. G. Li, et al. (Melville, NY: AIP), 75
Chapman, S. C., Hnat, B., Rowlands, G., & Watkins, N. W. 2005, Nonlinear Process. Geophys., 12, 767
Chechkin, A., & Gonchar, V. Y. 2000, Chaos Solitons Fractals, 11, 2379
Chui, C. K. 1992, An Introduction to Wavelets in Wavelet Analysis and its Applications (New York: Academic Press)
Coleman, P. J., Jr. 1968, ApJ, 153, 371
Daubechies, I. 1988, Commun. Pure Appl. Math., 41, 909
Dobrowolny, M., Mangeney, A., & Veltri, P. 1980, Phys. Rev. Lett., 45, 144
Dudok de Wit, T., & Krasnoselskikh, V. V. 1996, Nonlinear Process. Geophys., 3, 262
Elsässer, W. M. 1950, Phys. Rev., 79, 183

Farge, M. 1992, Annual Rev. Fluid Mech., 24, 395
Farge, M., Holschneider, M., & Colonna, J. F. 1990, in Topological Fluid Mechanics, ed. H. K. Moffat (Cambridge: Cambridge Univ. Press), 765
Farge, M., Schneider, K., & Devynck, P. 2006, Phys. Plasmas, 13, 042304
Feynman, J., & Ruzmaikin, A. 1994, J. Geophys. Res., 99, 17645
Forman, M. A. 2003, in AIP Conf. Ser., Vol. 679, Solar Wind Ten, ed. M. Velli, R. Bruno, F. Malara, & B. Bucci (Melville, NY: AIP), 550
Forman, M. A., & Burlaga, L. F. 2003, in AIP Conf. Ser., Vol. 679, Solar Wind Ten, ed. M. Velli, R. Bruno, F. Malara, & B. Bucci (Melville, NY: AIP), 554
Frisch, U. 1995, Turbulence. The legacy of A.N. Kolmogorov (Cambridge: Cambridge Univ. Press)
Galtier, S. 2006, J. Plasma Phys., 72, 721
Galtier, S., Pouquet, A., & Mangeney, A. 2005, Phys. Plasmas, 12, 092310
Goldreich, P. 2001, Ap&SS, 278, 17
Goldreich, P., & Sridhar, S. 1995, ApJ, 438, 763
Goldreich, P., & Sridhar, S. 1997, ApJ, 485, 680
Goldstein, B. E., Smith, E. J., Balogh, A., Horbury, T. S., Goldstein, M. L., & Roberts, D. A. 1995a, Geophys. Res. Lett., 22, 3393
Goldstein, M. L. 1995, in ESA Special Publication, Vol. 371, Proc. Cluster Workshops, Data Analysis Tools and Physical Measurements and Mission-Oriented Theory, ed. K.-H. Glassmeier, U. Motschmann, & R. Schmidt (Noordwijk: ESA), 137
Goldstein, M. L., & Roberts, D. A. 1999, Phys. Plasmas, 6, 4154
Goldstein, M. L., Roberts, D. A., & Matthaeus, W. H. 1995b, ARA&A, 33, 283
Goldstein, M. L., Roberts, D. A., & Matthaeus, W. H. 1997, in Cosmic Winds and the Heliosphere, ed. J. R. Jokipii, C. P. Sonett, & M. S. Giampapa (Tucson, AZ: Univ. Arizona), 521
Grappin, R., Leorat, J., & Pouquet, A. 1983, A&A, 126, 51
Grappin, R., Velli, M., & Mangeney, A. 1991, Ann. Geophys., 9, 416
Halsey, T. C., Jensen, M. H., Kadanoff, L. P., Procaccia, I., & Shraiman, B. I. 1986, Phys. Rev. A, 33, 1141
Hnat, B., Chapman, S. C., Kiyani, K., Rowlands, G., & Watkins, N. W. 2007, Geophys. Res. Lett., 34, 15108
Hnat, B., Chapman, S. C., Rowlands, G., Watkins, N. W., & Farrell, W. M. 2002, Geophys. Res. Lett., 29, 100000
Horbury, T. S. 1999, in Plasma Turbulence and Energetic Particles in Astrophysics, Proc. Int. Conf., ed. M. Ostrowski & R. Schlickeiser (Cracow: Uniwersytet Jagiellonski), 115
Horbury, T. S., & Balogh, A. 1997, Nonlinear Process. Geophys., 4, 185
Horbury, T. S., Balogh, A., Forsyth, R. J., & Smith, E. J. 1996, J. Geophys. Res., 101, 405
Horbury, T. S., Balogh, A., Forsyth, R. J., & Smith, E. J. 1997, Adv. Space Res., 19, 847
Horbury, T. S., Forman, M. A., & Oughton, S. 2005, Plasma Phys. Control. Fusion, 47, B703
Iroshnikov, P. S. 1963, AZh, 40, 742
Issautier, K., Meyer-Vernet, N., Moncuquet, M., Hoang, S., & McComas, D. J. 1999, J. Geophys. Res., 104, 6691
Jenkins, G. M., & Watts, D. G. 1968, Spectral Analysis and Its Applications, (New York: Holden Day, Inc.)
Jimenez, J., Wray, A. A., Saffman, P. G., & Rogallo, R. S. 1993, J. Fluid Mech., 255, 65
Katul, G., Vidakovic, B., & Albertson, J. 2001, Phys. Fluids, 13, 241
Katul, G. G., Albertson, J. D., Chu, C. R., & Parlange, M. B. 1994a, in Wavelets in Geophysics, ed. E. Foufoula Georgiou & P. Kumar (New York: Academic), 81
Katul, G. G., Geron, C. D., Hsieh, C. I., Vidakovic, B., & Guenther, A. B. 1998, J. Appl. Meteorology, 37, 1533
Katul, G. G., & Parlange, M. B. 1994, J. Atmospheric Sci., 51, 2181
Katul, G. G., Parlange, M. B., & Chu, C. R. 1994b, Phys. Fluids, 6, 2480
Kiyani, K., Chapman, S. C., & Hnat, B. 2006, Phys. Rev. E, 74, 051122
Kiyani, K. H., Chapman, S. C., & Watkins, N. W. 2009, Phys. Rev. E, 79, 036109
Kolmogorov, A. 1941, Akad. Nauk SSSR Dokl., 30, 301
Kolmogorov, A. N. 1962, J. Fluid Mech., 13, 82
Kraichnan, R. H. 1965, Phys. Fluids, 8, 1385
Leamon, R. J., Smith, C. W., Ness, N. F., Matthaeus, W. H., & Wong, H. K. 1998, J. Geophys. Res., 103, 4775
Leamon, R. J., Smith, C. W., Ness, N. F., & Wong, H. K. 1999, J. Geophys. Res., 104, 22331
Lepping, R. P., et al. 1995, Space Sci. Rev., 71, 207
Li, G. 2008, ApJ, 672, L65
Lin, R. P., et al. 1995, Space Sci. Rev., 71, 125
Mahrt, L. 1991, J. Atmospheric Sci., 48, 472
Mallat, S. G. 1989, in Wavelets, Time-frequency Methods and Phase Space, ed. J.-M. Combes, A. Grossmann, & P. Tchamitchian (Berlin: Springer), 313
Mangeney, A., Grappin, R., & Velli, M. 1991, in Advances in Solar System Magnetohydrodynamics, ed. E. R. Priest & A. W. Wood (Cambridge: Cambridge Univ. Press), 327
Mangeney, A., Salem, C., Veltri, P., & Cecconi, B. 2001, in ESA Special Publication, Vol. 492, Sheffield Space Plasma Meeting: Multipoint Measurements versus Theory, ed. B. Warmbein (Noordwijk: ESA), 53
Marsch, E. 1991, in Physics of the Inner Heliosphere. II. Particles, Waves and Turbulence, XI (Berlin: Springer), 159
Marsch, E., & Liu, S. 1993, Ann. Geophys., 11, 227
Marsch, E., & Tu, C. Y. 1994, Ann. Geophys., 12, 1127
Marsch, E., & Tu, C.-Y. 1997, Nonlinear Process. Geophys., 4, 101
Mason, J., Cattaneo, F., & Boldyrev, S. 2008, Phys. Rev. E, 77, 036403
Matthaeus, W. H., & Goldstein, M. L. 1982, J. Geophys. Res., 87, 6011
Meneveau, C. 1991a, J. Fluid Mech., 232, 469
Meneveau, C. 1991b, Phys. Rev. Lett., 66, 1450
Meyer, Y. 1989, in Wavelets, Time-Frequency Methods and Phase Space, ed. J.-M. Combes, A. Grossmann, & P. Tchamitchian (Berlin: Springer), 21
Meyer, Y. 1998, CRM Monograph Series, Vol. 9, Wavelets, Vibrations and Scalings (Providence, RI: American Mathematical Society), (x+133, with a preface in French by the author)
Meyer-Vernet, N., & Perche, C. 1989, J. Geophys. Res., 94, 2405
Mimouni, S., Laval, G., Scheurer, B., & Jaffard, S. 1995, in Lecture Notes in Physics, Vol. 462, Small-Scale Structures in Three-dimensional Hydrodynamic and Magnetohydrodynamic Turbulence, ed. M. Meneguzzi, A. Pouquet, & P.-L. Sulem (Berlin: Springer), 179
Mininni, P. D., Alexakis, A., & Pouquet, A. 2007, J. Plasma Phys., 73, 377
Moisy, F., & Jiménez, J. 2004, J. Fluid Mech., 513, 111
Müller, W.-C., & Biskamp, D. 2003, in Lecture Notes in Physics, Vol. 614, Turbulence and Magnetic Fields in Astrophysics, ed. E. Falgarone & T. Passot (Berlin: Springer), 3
Müller, W.-C., Biskamp, D., & Grappin, R. 2003, Phys. Rev. E, 67, 066302
Müller, W.-C., & Grappin, R. 2004, Plasma Phys. Control. Fusion, 46, B91
Müller, W.-C., & Grappin, R. 2005, Phys. Rev. Lett., 95, 114502
Muzy, J. F., Bacry, E., & Arneodo, A. 1993, Phys. Rev. E, 47, 875
Muzy, J. F., Bacry, E., & Arneodo, A. 1994, Int. J. Bifurcation and Chaos in Appl. Sci. Eng., 4, 245
Muzy, J. F., Bacry, E., & Kozhemyak, A. 2006, Phys. Rev. E, 73, 066114
Pagel, C., & Balogh, A. 2002, J. Geophys. Res. (Space Physics), 107, 1178
Pagel, C., & Balogh, A. 2003, J. Geophys. Res. (Space Physics), 108, 1012
Parisi, G., & Frisch, U. 1985, in Turbulence and Predictability in Geophysical Fluid Dynamics and Climate Dynamics, Proc. Int. School of Physics Enrico Fermi, June 1983, ed. M. Ghil, R. Benzi, & G. Parisi (Amsterdam: North-Holland (Italian Physical Society)), 84
Podesta, J. J. 2007, J. Geophys. Res. (Space Physics), 112, 11104
Podesta, J. J., Roberts, D. A., & Goldstein, M. L. 2006a, J. Geophys. Res. (Space Physics), 111, 10109
Podesta, J. J., Roberts, D. A., & Goldstein, M. L. 2006b, J. Geophys. Res. (Space Physics), 111, 9105
Podesta, J. J., Roberts, D. A., & Goldstein, M. L. 2007, ApJ, 664, 543
Roberts, D. A., & Goldstein, M. 1991, Rev. Geophys., 29, 932
Roberts, D. A., Goldstein, M. L., & Klein, L. W. 1990, J. Geophys. Res., 95, 4203
Roberts, D. A., Goldstein, M. L., Klein, L. W., & Matthaeus, W. H. 1987a, J. Geophys. Res., 92, 12023
Roberts, D. A., Goldstein, M. L., Matthaeus, W. H., & Ghosh, S. 1992, J. Geophys. Res., 97, 17115
Roberts, D. A., Klein, L. W., Goldstein, M. L., & Matthaeus, W. H. 1987b, J. Geophys. Res., 92, 11021
Ruzmaikin, A. A., Feynman, J., Goldstein, B. E., Smith, E. J., & Balogh, A. 1995, J. Geophys. Res., 100, 3395
Sahraoui, F. 2008, Phys. Rev. E, 78, 026402
Salem, C. 2000, PhD thesis, Univ. Paris VII
Salem, C., Bosqued, J.-M., Larson, D. E., Mangeney, A., Maksimovic, M., Perche, C., Lin, R. P., & Bougeret, J.-L. 2001, J. Geophys. Res., 106, 21701
Salem, C., Mangeney, A., Bale, S. D., Veltri, P., & Bruno, R. 2007, in AIP Conf. Ser., Vol. 932, in Turbulence and Nonlinear Processes in Astrophysical Plasmas, ed. D. Shaikh & G. P. Zank (Melville, NY: AIP), 75
Salem, C. S., Mangeney, A., & Bale, S. D. 2006, in AGU Fall Meeting Abstracts, 87, 52
Salem, C. S., Mangeney, A., Bale, S. D., & Veltri, P. 2004, AGU Fall Meeting Abstracts, C291
Sanderson, T. R., et al. 1998, J. Geophys. Res., 103, 17235
Sorriso-Valvo, L., Carbone, V., & Bruno, R. 2005, Space Sci. Rev., 121, 49
Sorriso-Valvo, L., Carbone, V., Giuliani, P., Veltri, P., Bruno, R., Antoni, V., & Martines, E. 2001, Planet. Space Sci., 49, 1193
Sorriso-Valvo, L., Carbone, V., Veltri, P., Consolini, G., & Bruno, R. 1999, Geophys. Res. Lett., 26, 1801

Sreenivasan, K. R., & Antonia, R. A. 1997, Annual Rev. Fluid Mech., 29, 435
Tu, C.-Y., & Marsch, E. 1995, Space Sci. Rev., 73, 1
Turiel, A., Yahia, H., & Pérez-Vincente, C. 2008, J. Phys. A: Math. Theor., 41, 015501
van Milligen, B. P., Sánchez, E., Estrada, T., Hidalgo, C., Brañas, B., Carreras, B., & García, L. 1995, Phys. Plasmas, 2, 3017
Veltri, P. 1999, Plasma Phys. Control. Fusion, 41, A787
Veltri, P. 2004, in AIP Conf. Ser., Vol. 703, Plasmas in the Laboratory and in the Universe: New Insights and New Challenges, ed. G. Bertin, D. Farina, & R. Pozzoli (Melville, NY: AIP), 133
Veltri, P., & Mangeney, A. 1999, in AIP Conf. Ser., Vol. 471, Solar Wind Nine, ed. S. R. Habbal, R. Esser, J. V. Hollweg, & P. A. Isenberg (Melville, NY: AIP), 543
Veltri, P., Nigro, G., Malara, F., Carbone, V., & Mangeney, A. 2005, Nonlinear Process. Geophys., 12, 245
Veltri, P., Carbone, V., Lepreti, F., & Nigro, G. 2009, in Encyclopedia of Complexity and Systems Science, ed. R. A. Meyers (Heidelberg: Springer), 8009
Vörös, Z., Baumjohann, W., Nakamura, R., Runov, A., Volwerk, M., Zhang, T. L., & Balogh, A. 2004, Phys. Plasmas, 11, 1333
Yamada, M., & Ohkitani, K. 1990, Prog. Theor. Phys., 83, 819